

Multi-Scale Characterization of Viscoelastic Properties in Structural Adhesives Using PZT Resonance and Non-Contact Impulse Validation

Serges Kikwani, Erick Ogam, Fréderic Lebon

▶ **To cite this version:**

Serges Kikwani, Erick Ogam, Fréderic Lebon. Multi-Scale Characterization of Viscoelastic Properties in Structural Adhesives Using PZT Resonance and Non-Contact Impulse Validation. Results in engineering, 2025, pp.108035. ⟨10.1016/j.rineng.2025.108035⟩. ⟨hal-05354634⟩

HAL Id: hal-05354634

https://cnrs.hal.science/hal-05354634v1

Submitted on 16 Apr 2026

HAL is a multi-disciplinary open access archive for the deposit and dissemination of scientific research documents, whether they are published or not. The documents may come from teaching and research institutions in France or abroad, or from public or private research centers.

L'archive ouverte pluridisciplinaire **HAL**, est destinée au dépôt et à la diffusion de documents scientifiques de niveau recherche, publiés ou non, émanant des établissements d'enseignement et de recherche français ou étrangers, des laboratoires publics ou privés.



Distributed under a Creative Commons CC BY 4.0 - Attribution - International License

Journal Pre-proof

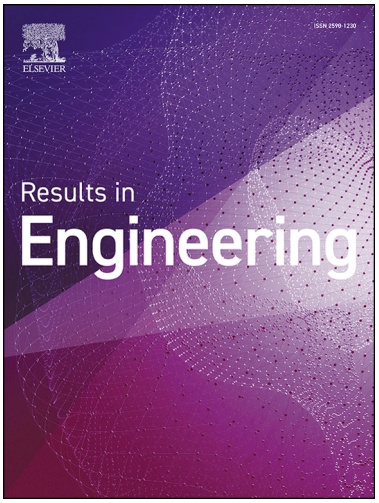

Multi-Scale Characterization of Viscoelastic Properties in Structural Adhesives Using PZT Resonance and Non-Contact Impulse Validation

Serges Kikwani, Erick Ogam and Fréderic Lebon

PII: S2590-1230(25)04085-X
DOI: https://doi.org/10.1016/j.rineng.2025.108035
Reference: RINENG 108035

To appear in: *Results in Engineering*

Received date: 12 August 2025
Revised date: 18 October 2025
Accepted date: 1 November 2025

Please cite this article as: S. Kikwani, E. Ogam and F. Lebon, Multi-Scale Characterization of Viscoelastic Properties in Structural Adhesives Using PZT Resonance and Non-Contact Impulse Validation, *Results in Engineering*, 108035, doi: https://doi.org/10.1016/j.rineng.2025.108035.

This is a PDF of an article that has undergone enhancements after acceptance, such as the addition of a cover page and metadata, and formatting for readability. This version will undergo additional copyediting, typesetting and review before it is published in its final form. As such, this version is no longer the Accepted Manuscript, but it is not yet the definitive Version of Record; we are providing this early version to give early visibility of the article. Please note that Elsevier's sharing policy for the Published Journal Article applies to this version, see: https://www.elsevier.com/about/policies-and-standards/sharing#4-published-journal-article. Please also note that, during the production process, errors may be discovered which could affect the content, and all legal disclaimers that apply to the journal pertain.

© 2025 Published by Elsevier.

Highlights

- Non-destructive RUV technique measures stiffness and damping in adhesives.
- Non-contact impulse and vibrometer tests validate low-frequency behavior.
- A quadratic damping model is developed from viscoelasticity theory.
- The model is validated in a high-frequency regime above 200 kHz.
- Six adhesives are characterized to support dynamic material selection.

Journal Pre-proof

Multi-Scale Characterization of Viscoelastic Properties in Structural Adhesives Using PZT Resonance and Non-Contact Impulse Validation

Serges Kikwani[a], Erick Ogam[a], Fréderic Lebon[a]

[a]*Aix Marseille Univ, CNRS, Centrale Med, LMA, Marseille, 4 impasse Nikola Tesla, CS 40006,13453 Marseille, France*

Abstract

Technical datasheets for structural adhesives, such as epoxies, methacrylates, and polyurethanes, typically report static elastic moduli but rarely include Poisson's ratios or damping characteristics, which are essential for applications involving dynamic or vibratory loading. This study presents a non-destructive methodology for determining the dynamic Young's modulus, Poisson's ratio, and damping properties using resonant ultrasonic vibration (RUV) combined with inverse finite element analysis.

Experimental data from six structural adhesives revealed a quadratic relationship between the damping coefficient and the ratio of dynamic to static Young's moduli. This behavior was found to be consistent with a viscoelastic representation based on the Kelvin–Voigt mechanical model and scaling principles from the Doi-Edwards theory for entangled polymer networks. The resulting model expresses the storage modulus as a quadratic function of the damping ratio and is validated in a high-frequency regime above 200 kHz, where strain rates are significantly elevated.

*Corresponding author. E-mail: kikwani@lma.cnrs-mrs.fr (S. Kikwani)

Journal Pre-proof

Journal Pre-proof

To complement the RUV tests, transient mechanical impulse excitation and non-contact laser vibrometer velocity measurements were conducted on larger specimens to capture lower-frequency modes. This multi-scale characterization strategy enabled validation of resonance frequencies and extended the applicability of the model. Among the adhesives tested, Sikadur 30 exhibited the highest stiffness, whereas 3M 2216 showed the lowest. 3M 2216 also demonstrated the greatest damping capacity, while Sicomin presented the lowest stiffness. Araldite and 3M 2216 displayed the highest Poisson's ratios, while the other adhesives (Loctite, SAF 30, Sicomin, and Sikadur 30) showed comparably low values. In terms of modulus ratio, SAF 30 recorded the highest value, whereas Sicomin exhibited the lowest. Additionally, glass transition temperature (T_g) measurements clarified that the adhesives with the lowest stiffness corresponded to those with the lowest T_g, linking reduced rigidity to lower transition temperatures.

The proposed model, fitted to the modulus-to-damping ratio data, offers a framework for selecting structural adhesives in applications requiring both mechanical strength and vibrational energy dissipation.

Keywords: Structural Adhesives, Young's Modulus, Poisson's Ratio, Resonant Ultrasonic Vibration, Damping Coefficient, Modulus Ratio.

1. Introduction

In recent decades, structural bonding technologies have gained ground in the aerospace sector [1, 2] thanks to advances in the development of high-performance materials and the need for lighter structures. Structural bonding is a suitable joining method for composite materials that are typically used

Journal Pre-proof

for these structures [2, 3, 4, 5, 6]. Recent advances in this field have led to their use in the automotive [7, 8, 9], marine [10, 11], and civil engineering sectors [12]. These technologies are affordable and competitive compared to conventional technologies such as riveting. The aim is to reduce the weight of the final structures [10, 13] and ensure their durability by resisting corrosion while maintaining good mechanical performance. However, these techniques still suffer from a lack of knowledge in terms of sizing, service life, e.t.c.

The objective of this study is to develop methods for determining the dynamic Young's moduli and Poisson's ratios of structural adhesives, and to identify the viscoelastic behavior law that best describes their response. Structural adhesives are frequently used in applications subject to shock and vibration, where an accurate understanding of their dynamic mechanical behavior is essential. However, technical datasheets for these materials—such as epoxies, methacrylates, and polyurethanes—typically provide only static elastic moduli and rarely include Poisson's ratios or damping characteristics. This lack of dynamic mechanical data, particularly Poisson's ratio, constitutes one of the main motivations of the present study.

The RUV test is a non-destructive method used to determine the dynamic elastic properties of materials at room temperature. Each specimen exhibits specific resonance frequencies that depend on its elastic modulus, mass, and geometry. By accurately measuring the specimen's geometry, mass, and resonance frequencies—typically for shapes such as rectangular beams, disc-like samples, or cylindrical rods : the dynamic elastic moduli [14] and damping coefficients can be determined.

A quadratic viscoelastic model is proposed, grounded in the Kelvin–Voigt

Journal Pre-proof

mechanical representation and the Doi–Edwards theory for entangled polymer networks.

The ultimate goal is to evaluate which materials conform to the proposed model and to identify those best suited for applications requiring both stiffness and vibration damping. These results will also be able to complement the technical data sheets of the adhesives as well as some already published works by providing, on the one hand, information on the Poisson's ratio and damping coefficients of these six adhesives and, on the other hand, a precise idea of the behavior (elastic or viscoelastic) of these six different adhesives from their Young's moduli ratio and their damping coefficients.

Another non-destructive approach involves dynamic mechanical measurements, in which the modulus, damping, or both are determined while the specimen is subjected to a controlled force or displacement. These properties are measured as functions of temperature, frequency, time, or a combination of these variables [14].

The excitation force in dynamic tests can be a dynamic shock [1], an impulse vibration [15, 16], an impact-echo [16, 17, 18], harmonic excitation. In this study, we employed two techniques of excitation, a harmonic steady state and mechanical impulse excitation. The latter was for comparison purposes.

In the standard test method, the dynamic Young's modulus and Poisson's ratio are obtained from the frequencies of the first two longitudinal (compressional) vibration resonance modes. The frequency range specified in the ASTM E1876 standard test method requires a sensor with a bandwidth of approximately 100 Hz to 50 kHz [14].

Journal Pre-proof

ASTM E1876 is limited to 50 kHz and assumes simple beam/rod geometries, while our disc adhesives resonate up to above 200 kHz.

This presents a significant limitation in our study, as the measured resonance frequencies exceed 200 kHz. Another constraint arises from the standard's requirement that specimens have specific geometries, typically rods with circular sections or rectangular beams, ensuring well-defined modal characteristics. To overcome these limitations, we employ a three-dimensional finite element modeling approach combined with inverse problem-solving techniques, allowing for accurate analysis of arbitrary sample geometries and higher-frequency responses.

For the selection of adhesives to be studied, we reviewed the work of A. Maurel-Pantel et al. [1], who compared the static test and dynamic impact tests properties of Araldite AV138M-1/HV998, 3M Scotch-Weld 2216 B/A, and Permabond 910 adhesives for space optics applications. A special experimental setup was developed for their study. In that work, with respect to static tests, the average fracture load was measured and a point stress criterion was proposed to determine the critical stress of adhesives in traction and shear. However, for impact tests, the impact strength of the adhesives was tested in traction and shear configurations thanks to the integration of the arcan fixture. K. Idrissa et al. [10] compared the durability of Sikadur 30 and Loctite UK 1351 B25 adhesives for bonding secondary structure applications in offshore wind turbines, using static tensile tests. Young's moduli of adhesives depend on curing temperatures. Whenever temperatures are involved, dynamic mechanical analysis (DMA) is employed. R. J. C. Carbas et al. [19] described the influence of improved curing temperature on the physical and

Journal Pre-proof

mechanical properties (Young's modulus and elastic limit) of the adhesives, Araldite 2011, Araldite AV138M-1/HV998 and Sikadur 30 LP) using DMA.

The influence of temperature on the resonance frequencies of three epoxy resins were studied in reference [20] : Araldite AV138-2BR/HV998, Fusor 380 NS/383 NS, and Araldite. Prof. (A)/Ar. Prof. (B). They were employed to attach transducers to structures. The electromechanical impedance of sensors attached to an aluminium sheet using these epoxy resins was monitored alongside estimations of the degree of cure from differential scanning calorimetry (DSC). The results showed that the resonance frequencies were displaced by up to 30 kHz and that the amplitudes changed considerably during the curing process of the selected resins. Y.Y. Lim et al. [21]. monitored the curing process of Sikadur 330 (the initial setting and subsequent curing process) using the electromechanical impedance technique (EMI). This involved employing an intelligent piezoelectric material embedded in an epoxy sample in a liquid state. The authors examined the relationship between the conductance signatures and the frequency, as well as the resonance frequency of the first PZT peak and the adhesive time.

The RUV testing using piezoelectric transducers is now well established and reliable method to determine the Young moduli and Poisson ratios [22, 23, 24, 25].

The dynamic Young's moduli values of materials obtained from vibrational tests can be different from those obtained in static tensile tests. Here are some of the effects that can cause variability :

- Strain rate effects on adhesives : The RUV tests assume loading at high frequencies, which corresponds to a high strain rate. Adhesives may

Journal Pre-proof

exhibit higher apparent stiffness (higher Young's modulus) at higher strain rates because they have less time to deform, effectively resisting deformation. In vibration tests (dynamic tests), the strain rate is related to the applied strain, which often varies sinusoidally with time. The strain as a function of time (t) can be expressed by

$$\varepsilon(t) = \varepsilon_0 \sin(\omega t), \tag{1}$$

where ε_0 is the strain amplitude, $\omega = 2\pi f$ (f is the frequency) is the angular frequency.

The strain rate in vibration [26] is given by

$$\dot{\varepsilon}_v(t) = \frac{d\varepsilon(t)}{dt} = \varepsilon_0 \omega \cos(\omega t). \tag{2}$$

Static tensile tests assume much lower strain rates, which allows more time for the adhesive to undergo deformation, this can result in low apparent stiffness (lower Young's modulus). The strain rate in static tensile is given by

$$\dot{\varepsilon}_{\text{static}} = \frac{\Delta \varepsilon_s}{\Delta t} \tag{3}$$

In displacement-controlled static tests, the strain rate is typically calculated using the crosshead speed v and the original gauge length of the specimen. The deformation rate in static tension becomes :

$$\dot{\varepsilon}_{\text{static}} = \frac{v}{L_0} \tag{4}$$

Journal Pre-proof

- Effects of viscoelastic properties of adhesives : Adhesive moduli depend on the way they are loaded (loading rate). For high frequencies, such as those of the RUV tests, Young's modulus are higher because both elastic and viscous components contribute to the deformation unlike in static tensile tests. The ratio R_E between the Young's modulus in vibration tests, E_{v} and that in static tensile tests E_{static}, indicates the degree of viscoelastic dependence (sensitivity to the excitation frequency) of the adhesive and are evaluated using

$$R_E = \frac{E_{\mathrm{v}}}{E_{\mathrm{static}}}. \tag{5}$$

  If $R_E \sim 1$, the adhesive has a purely elastic behavior, its Young's modulus is independent of the frequency and this is the case with metals. If $R_E > 1$, the adhesive has a viscoelastic behavior, it appears more rigid in vibration than in static tensile, because it does not have time to deform plastically. Herein, the modulus ratios wee derived from elastic and damping properties identified through resonant ultrasonic vibration (RUV) [22, 23, 24, 25, 27] measurements, in conjunction with static tensile test results available in the literature.

- Damping effects of adhesives and internal friction : At high frequencies, such as in RUV testing, energy losses due to internal friction or damping within materials can lead to increased stiffness. These effects are less pronounced in static testing. The damping coefficient, ζ (quantifies the energy dissipation), is determined for light damping ($\zeta < 0.1$) by a simple one mode method [28] (used herein for simplicity):

Journal Pre-proof

$$\zeta = \frac{\Delta_f}{2f_{\max}^{\exp}}, \tag{6}$$

where Δf is the width of the resonance peak (at mid-amplitude), $f_{\max}^{\exp}$ is the resonance frequency of experimental RUV spectra. A broad resonance peak indicates high damping, that is, a high energy dissipation in the material. If ζ is large, the material is highly damped, meaning that it quickly dissipates mechanical energy in the form of heat or through other internal mechanisms. The amplitude of the vibrations decreases rapidly. A material with a large ζ is often used in applications where it is desired to attenuate or reduce vibrations, such as in shock absorbers or materials used in structures where it is essential to limit vibrations. If ζ is small, this means that the material is poorly damped, that is, it retains vibration energy better and the vibrations persist longer. A material with a low ζ is often used in situations where transmission of vibrational energy is desired, such as in some ultrasonic sensors, or in applications where it is desired that the adhesive retain its mechanical properties for a long time without too much energy loss.

Knowledge of the dynamic properties of aerospace bonded joints is essential, since accurate characterization of damping enables the reduction of vibration-induced fatigue. An aircraft's wings are subjected to fluctuating aerodynamic loads during flight. Resonance with the wing's flexural frequency can cause aerodynamic flutter, leading to potentially catastrophic dynamic instability. In automotive, the mechanical properties of the adhesives must be evaluated in order to determine their ability to withstand vibrations; In wind turbines, in addition to bonding secondary structures,

Journal Pre-proof

these adhesives must withstand the vibrations generated during operation. Adhesives in bionic systems enable the reliable bonding of soft materials to rigid electronic components, while also ensuring biocompatibility and resistance to mechanical stresses encountered in dynamic biological environments [29, 30, 31, 32].

This manuscript presents a scientifically rigorous and experimentally validated methodology for characterizing structural adhesives under dynamic loading conditions and introduces a novel non-contact approach that combines RUV and inverse finite element modeling to measure E_v, ν_v (Poisson's ratio in vibration), and ζ for six structural adhesives. The measured parameters were validated via impulse excitation, and a quadratic relationship between R_E and ζ was established. Furthermore, glass transition temperature (T_g) experiments were conducted, revealing that the adhesives exhibiting the lowest stiffness also possessed the lowest T_g, thereby linking reduced rigidity to lower transition temperatures.

2. Materials and preparation

2.1. Studied Adhesives

The choice of adhesives depends on the thermal, mechanical and environmental constraints associated with the intended applications. Table 1 lists some of the properties of the adhesive families studied.

Journal Pre-proof

Properties	**Epoxide**	**Acrylic or Methacrylate**	**Polyurethane**
Glass transition temperature (T_g)	75°C [33], 190°C [34]	105°C [35], 59 - 117°C [33]	30 - 120°C [36]
Flexibility	Low	Medium	High
Chemical resistance	Excellent	Medium	High
Moisture resistance	Good	Good	Very good
Adhesion	Excellent	Good	Very good
Curing time	Long	Fast	Medium
Mechanical resistance (Stiffness)	Excellent	Medium	Low

Table 1: Properties of adhesives in relation to their classification

For this work, Loctite UK 1351 B25, Saf 30 MIB, Sicomin SR 5030, Araldite AV138M-1/HV998, 3M Scotch-Weld 2216 B/A and Sikadur 30 adhesives were chosen on the basis of their availability. The technical data sheets for the selected adhesives were found to lack Poisson ratios and damping coefficients. Static Young's moduli (tensile), on the other hand, are the most widely available elastic properties.

2.1.1. Loctite UK 1351 B25 Adhesive (Henkel Adhesive Technologies, Düsseldorf, Germany).

This is a solvent-free, two-component, polyurethane-based adhesive for structural bonding. The resin (part A) contains organic compounds with hydroxyl groups, the hardener (part B) is isocyanate-based. The two components were mixed and the resulting structural adhesive is green in color, capable of filling gaps of up to 15 mm. The smaller sample size are noted as LC-S-1, LC-S-2 and LC-S-3 and the larger sample size as LC-L-1, LC-L-2 and LC-L-3.

Journal Pre-proof

2.1.2. Saf 30 MIB Adhesive (Bostik, France)

A two-component methacrylate adhesive offers unrivalled performance in terms of strength and flexibility, it is designed for use at temperatures between +12°C and +35°C to bond a wide range of dissimilar substrates such as metals and plastics, as well as composite materials for industrial applications. These exceptional properties enable structural bonding while maintaining flexibility and fatigue resistance. It withstands the most aggressive environments and extreme temperatures. The two components have been blended and the structural adhesive formed is beige in color, turning yellow over time. The smaller sample size are noted as SF-S-1, SF-S-2 and SF-S-3 and the larger sample size as SF-L-1, SF-L-2 and SF-L-3.

2.1.3. Sicomin SR 5030 Adhesive (Sicomin, Châteauneuf les Martigues, France)

This two-component epoxy adhesive is used for structural bonding and fillet joints. It is characterized by good mechanical strength and high thixotropy for good vertical hold. The two components have been mixed and the resultant structural adhesive is green in color, formulated for vertical and overhead bonding, as well as for joints up to 50 mm gap, even if the parts are immediately post-cured at high temperatures (up to 80°C). The smaller sample size are noted as SC-S-1, SC-S-2 and SC-S-3 and the larger sample size as SC-L-1, SC-L-2 and SC-L-3.

2.1.4. Araldite AV138M-1/HV998 Adhesive (Huntsman, UK)

This is a two-component adhesive, consisting of an epoxy resin and a hardener, curing at room temperature. The process can be accelerated by heat treatment. Once fully cured, the adhesive exhibits excellent behavior

Journal Pre-proof

at high temperatures and high resistance to chemicals. Suitable for bonding a wide variety of metals, ceramics, glass, rubbers, rigid plastics and other materials, it is used in many industrial applications where resistance to aggressive environments or high temperatures is required. The smaller sample size are noted as AR-S-1, AR-S-2 and AR-S-3 and the larger sample size as AR-L-1, AR-L-2 and AR-L-3.

2.1.5. 3M2216 Scotch-Weld 2216 B/A Adhesive (3M Company, France)

This is a two-component adhesive consisting of an epoxy resin and an aliphatic diamine hardener. The final mixture is gray in color. After mixing these two components. The process can be accelerated by heat treatment. The adhesive can be used for applications in aircraft and aerospace vehicles. The smaller sample size are noted as 3M-S-1, 3M-S-2 and 3M-S-3 and the larger sample size as 3M-L-1, 3M-L-2 and 3M-L-3.

2.1.6. Sikadur 30 Adhesive (Sika France SAS, France)

This is a two-component adhesive, a blend of epoxy resin and special fillers. It is designed for use at temperatures between +8°C and +35°C. It polymerizes over time. The two components have been mixed and the structural adhesive formed is light gray in color. The smaller sample size are noted as SK-S-1, SK-S-2 and SK-S-3 and the larger sample size as SK-L-1, SK-L-2 and SK-L-3.

2.2. Manufacturing of Molds and Preparation of Adhesives

Specimens of the adhesives were specifically designed for vibratory characterization, with two types of cylindrical disc-like samples fabricated for different measurement techniques. Smaller diameter samples, with dimensions

Journal Pre-proof

of (18 ± 0.2) mm in diameter and (6 ± 0.2) mm in thickness (Geometry is given in Fig. 1 and Appendix B), were used for resonant ultrasound vibration (RUV) measurements (Small discs for RUV to access high-frequency resonances). Larger diameter samples were prepared for mechanical impulse time-domain measurements (larger discs (50 mm x 10 mm) for impulse excitation at low frequencies). A tolerance was allowed in the mold dimensions to account for the Teflon adhesive film used for demolding.

All adhesives are two-component systems and were prepared according to the proportions in Table 3. In the absence of a standard protocol to control adhesive porosity, the mixtures were stirred for 3 minutes at low speed to minimize air bubbles and voids, until a homogeneous consistency, as recommended by the technical datasheets, was achieved, except for Loctite and Saf 30, for which dispensing guns were used.

Three samples per type of adhesive were made to evaluate the dispersion of the measurements. The cured adhesive samples were subjected to dynamic loading, and their elastic properties and damping were subsequently determined.

When manufacturing samples, the influence of the uncertainties of the measurement parameters (sample dimensions) on the elastic parameters (Young's modulus and Poisson's ratio) to be determined must be taken into account[14]. Table 2 shows that calculations are particularly sensitive to measurement errors in the thickness of samples, hence the use of 3D printed molds. Special attention must be paid to the measurement of sample thicknesses less than 3 mm[14].

Journal Pre-proof

Variable	Measurement Error	Variable Exponent in Modulus Equation	Calculation Error
Frequency (f)	0.1%	f^2	0.2%
Length (L)	0.1%	L^3	0.3%
Mass (m)	0.1%	m	0.1%
Width (b)	0.1%	b^{-1}	0.1%
Thickness (t)	0.1%	t^{-3}	0.3%
Diameter (D)	0.1%	D^{-4}	0.4%

Table 2: Effects of Variable Error on Modulus Calculation [14].

Sample molds were designed using SolidWorks [37] (Dassault Systems, France), then manufactured by 3D printing in a Raise 3D N2 Plus Dual printer (Raise 3D, China), using 1.75 mm diameter PLA+ (Polylactic acid) plastic filaments. The surfaces of the molds were then coated with Teflon adhesive tape to facilitate demolding of the adhesives samples after curing. Fig.1 shows the CAD (Computer-Assisted Design) model of the mold and its dimensions.

The adhesive mixtures were prepared according to the instructions in the adhesive data sheets. Table 3 lists the dosages, curing times, and components (resin and hardener) used to prepare the adhesives.

Journal Pre-proof

Journal Pre-proof

Specification	Loctite	Saf 30	Sicomin	Araldite	3M2216	Sikadur 30
Type	Polyurethane	Methacrylate	Epoxy	Epoxy	Epoxy	Epoxy
Resin	UK 1351 B25	Comp A	Isobon SR 5030	AV 138M-1	2216 - Comp B	Sika - Comp A
Hardener	UK 5452	Comp B	Isobon SD 5032	HV998	2216 - Comp A	Sika - Comp B
Mixing Method	Gun	Gun	Manual	Manual	Manual	Manual
Curing Time	24h at 23°C	24h at 23°C	-	24h at 23°C	7 days at 24°C	48h at 23°C
Resin/Hardener Ratio	10/4 g	2/1 ml	10/4.5 g	10/4 g	5/7 g	4.5/1.5 g

* Missing values (-) indicate in the data sheet.

Table 3: Composition, mixing methods, curing conditions, and resin-to-hardener ratios for the preparation of the studied adhesives.

Adhesives were prepared in a conditioned room, at a controlled temperature of 23°C, relative humidity of (50±5)%, and atmospheric pressure. After 24 hours' exposure, the samples were demolded, releasing the two side curved walls of the mold through the four notches made in the contour of the mold base, as shown in Fig.1.

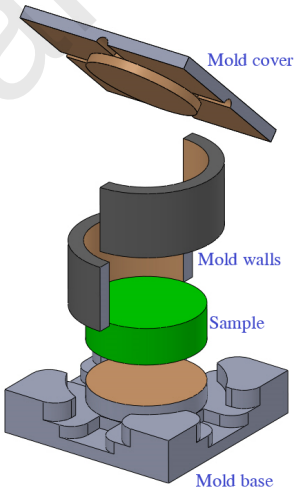

Figure 1: 3D SOLID WORKS mold and Adhesive (Demolding sequence)

Journal Pre-proof

Specimen surfaces were meticulously prepared, as shown in Fig.2, to ensure optimal piezoelectric transducer mounting. Opposing faces were manufactured round, parallel, with a constant diameter. Table 4 shows curing schedules, curing time and data glass transition values of the studied adhesive samples.

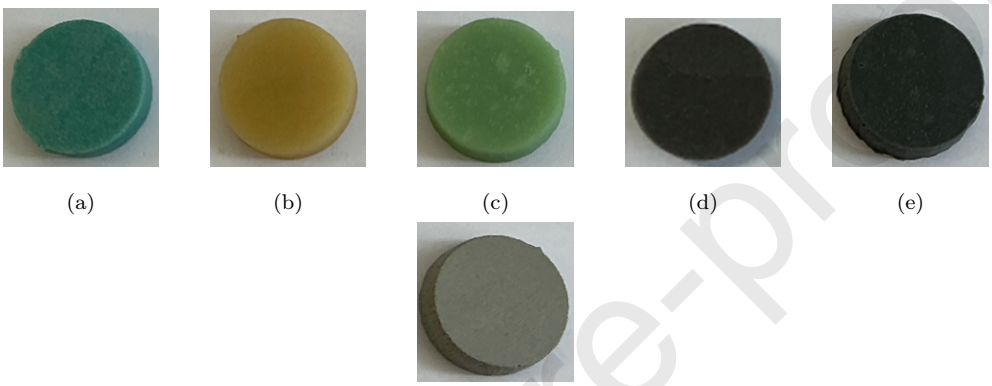

(a) (b) (c) (d) (e) (f)

Figure 2: Photograph of the prepared adhesive samples: (a) Loctite UK 1351 B25; (b) Saf 30 MIB; (c) Sicomin SR5030; (d) Araldite AV138M-1/HV998; (e) 3M Scotch-Weld 2216 B/A; and (f) Sikadur 30.

	Loctite	**Saf 30**	**Sicomin**	**Araldite**	**3M2216**	**Sikadur 30**
Curing schedules before demolding at 23°C (Days)	1	1	1	1	1	1
Curing Time at 23°C (Days)	19	21	20	21	14	11
Age distribution from demolding to testing (Days)	19	21	20	21	14	11
Data sheet Glass transition values T_g (°C)	79	-	82	-	-	50

No indicated values in data sheet (-).

Table 4: Curing schedules, curing time and data glass transition values of the studied adhesive samples.

Journal Pre-proof

3. Methods

3.1. Measurements of the densities of the various adhesive samples studied

The density of the adhesive samples was evaluated using

$$\rho_{\mathrm{s}} = \frac{M_A}{M_A - M_W} (\rho_{\mathrm{w}} - \rho_{\mathrm{a}}) + \rho_{\mathrm{a}} \tag{7}$$

Where ρ_{w} is the density of distilled water and ρ_a is the density of air, M_A represents the mass of the sample measured in the open air, and M_W its mass after immersion in a distilled water bath (used as a reference liquid). M_A and M_W were measured using the OHAUS densitometer balance (Nänikon, Switzerland). M_A and M_W were calculated from the average of five measurements to ensure accurate results. The densitometer is equipped with a precision balance accurate to 10^{-3} grams.

3.2. Experimental Methods

3.2.1. Resonant Ultrasound Vibration Test

The RUV testing setup follows previously published works by the authors [22, 24, 23, 25]. Cylindrical adhesive samples were tested using two 12 mm PZT piezoelectric transducers (the ceramic element of Kingstate KPEG 110, Taipei, Taiwan), one acting as an exciter and the other as a sensor. These were bonded on opposite faces of the sample using thin double-sided adhesive tape to ensure consistent contact.

The harmonic excitation signal was generated by a Lock-in Amplifier (Signal Recovery 7265 DSP, Oak Ridge, TN, USA), amplified by an integrated audio amplifier (Cambridge Audio AXA35, London, United Kingdom), and

Journal Pre-proof

the sensor signal was further amplified using a low-noise amplifier (NF SA-200F3, Yokohama, Japan) powered by a DC supply (NF SA-91521, Yokohama, Japan).

The excitation frequency ranged from 10 kHz to 250 kHz in 100 Hz steps, targeting compressional vibration modes. Environmental conditions such as temperature (approx. 25°C) and pressure were controlled. Repeatability tests showed no significant deviation in the spectra.

3.2.2. Mechanical Impulse loading, non-contact laser vibrometer velocity measurements

To validate and compare the RUV results to those obtained at lower frequencies (audible and ultrasonic range), time-domain mechanical impulse loading were performed on larger adhesive samples (50 mm diameter, 10 mm thickness) as shown in the schematic diagram in Fig 3. and on the experimental set up in Fig. 4. A 27 mm diameter PZT ceramic disc (extracted from a Kingstate KPEG827 buzzer, Taipei) was used as the ultrasonic actuator. It was connected to a waveform generator (Agilent 33220A, Santa Clara, CA, USA) and driven through an amplifier (Cambridge Audio AXA35, Cambridge, United Kingdom). The transient mechanical excitation (Rectangular impulse signal, width 15 μs) was applied to one face of the sample, while the vibrational response was measured on the opposite face using a non-contact laser vibrometer, consisting of a sensor head (Polytec OFV-505/503, Waldbronn, Germany) and controller (Polytec OFV-5000-S, Waldbronn, Germany).

This laser vibrometer system enables high-precision, non-contact velocity measurements, minimizing the risk of interfering with the sample's dynamic

Journal Pre-proof

response.

Signal acquisition was carried out using a high-resolution digitizer (National Instruments PXI-5922, Austin, TX, USA). Temporal response signals were processed using Fast Fourier Transform (FFT), and the spectrum was limited to the 0–50 kHz range, in accordance with the vibration testing standard [14]. The first two compressional modes were identified and compared with those predicted using the Young's modulus and Poisson's ratio values obtained from the RUV measurements.

This complementary test not only verifies the RUV results but also provides additional data in the lower frequency range using a different, contactless measurement approach.

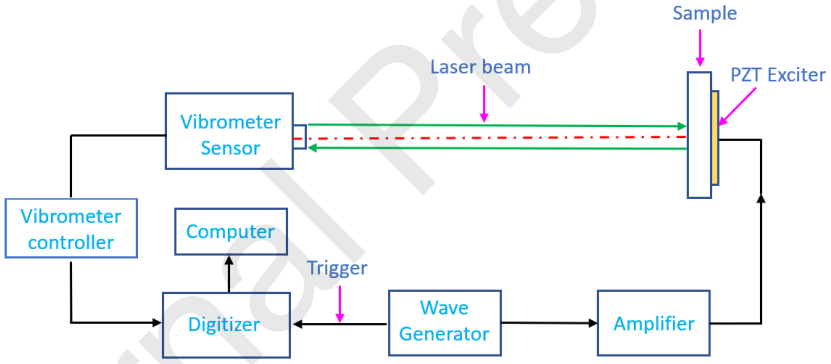

Figure 3: Schematic diagram of the experimental set up of Impulse test using Laser Vibrometer head Sensor

Journal Pre-proof

Journal Pre-proof

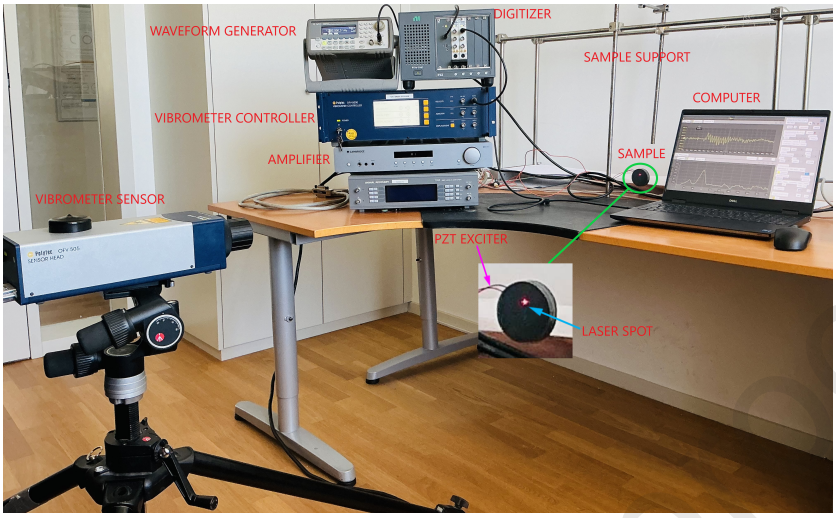

Figure 4: Experimental set up of Impulse test using Laser Vibrometer head Sensor

3.3. Vibrational modal analysis to identify mode shapes in measured RUV spectra and recovery of provisional Young's moduli and Poisson's ratios

The results of the vibrational modal analysis of the smaller samples were used to identify the dynamic properties of the structure, i.e. its natural frequencies and associated deformation modes. E. Ogam et al. [25] have confirmed in their work that it is difficult to accurately identify the natural modes of vibration that correspond to the resonance frequency observed by spectrum measurements for several reasons, such as: mode coupling, difficulties in distinguishing the different types of modes (Compressional, bending and torsional, etc.) and the presence of noise, they suggested always choosing sample geometries likely to provide a vibration spectrum with well-separated resonance peaks. The provisional Young's moduli and Poisson's ratios (E_p, ν_p) were identified using the measured spectra and 3D numerical modal analysis performed with the finite element method (FEM), implemented in COMSOL

Journal Pre-proof

Multiphysics [38] and ABAQUS [39].

Only compressional peaks confirmed by FEM were selected. In order to avoid bending or torsional coupling, and to favor longitudinal modes, the excitation was applied axially (perpendicular to the surface of the disc).

COMSOL was selected for its ease of integration with MATLAB, which facilitates the solution of the inverse problem, while ABAQUS was used for comparative verification. A 3D FEM modal analysis of the sample model was conducted using the settings shown in Table 5. E_p and ν_p were adjusted in ABAQUS until the first two natural compressional modes of the 3D vibrational numerical FEM analysis corresponded to the peaks of the experimentally measured RUV spectra. These values are called provisional.

Since the adhesive samples under study may contain closed pores (external or internal pores that do not interconnect), it is assumed, within the framework of the 3D FEM used for modal identification and dynamic analysis, that the samples behave as equivalent solid, with homogeneous and isotropic properties. Accordingly, the presence of voids and entrapped air bubbles were neglected in the model.

Settings	**ABAQUS 2021**	**COMSOL Multiphysics 6.1**
Analysis Type	Modal analysis	Modal analysis
Boundary Conditions	No constraints applied	No constraints applied
Element Type	C3D20R (64985, 20-node quadratic hexahedral element)	3D quadratic tetrahedral element
Meshing Method	Manual (partitioning + seeding)	Free tetrahedral mesh
Approximate global Size	0.0005	Predefined size: Thinner (max: 0.00099, min: 0.000072)

Table 5: Summary of some settings used for modal vibration analysis of 3D FEM of adhesive samples studied (ABAQUS 2021 software and COMSOL software version 6.1)

Journal Pre-proof

3.4. Optimization of Young's modulus and Poisson's ratio values

The final (optimal) Young's moduli and Poisson ratios (E_v, ν_v) of the adhesives were determined using a cost function. This function was based on the first two natural compressional modes obtained from 3D numerical FEM analysis (COMSOL Multiphysics) and the corresponding experimental resonance frequencies from the RUV spectra. As in the work of E. Ogam et al. [25], the cost function $\mathcal{J}(E_v, \nu_v)$ is defined as:

$$\mathcal{J}(E_v, \nu_v) = \sum_{n=1}^{2} \omega_n^2 \left[f_{\text{exp}}^n - f_{\text{mode}}^n(E_v, \nu_v) \right]^2 \tag{8}$$

where ω_n is the mode weighting coefficient, set to 1 when all modes receive equal weight [25]. Here, f_{exp}^n represents the experimental resonance frequencies, while f_{mode}^n are the natural vibrational modes obtained from 3D FEM analysis for the current trial values of (E_v, ν_v).

Since the problem is ill-posed and allows multiple solutions, the optimization process is performed iteratively. The solution that minimizes the cost function is found automatically using a non-linear Nelder-Mead optimization algorithm [40]. This algorithm provides the solutions in terms of the values of the minima of the cost function. Optimization was carried out by coupling MATLAB [41] with COMSOL Multiphysics [38]. The optimal solution was selected from the 3D cost function curve of E_p and ν_p, corresponding to the minimum of the cost function. (The setting details are given in Appendix C).

Journal Pre-proof

3.5. Confrontation of experimental RUV spectra with 3D Numerical RUV Spectra of Steady-State Finite Elements Method (ABAQUS)

A steady-state 3D finite element dynamic study was employed to calculate the vibration spectrum, assuming the adhesives were homogeneous, isotropic, and elastic without damping.

The 3D model was excited using a harmonic force applied at the center, which matches the diameter of the piezoelectric discs. This setup replicated the experimental mounting of the discs on physical adhesive samples. A 3D FEM Steady-State analysis of the sample model was conducted using the settings shown in the Table 6 [24, 25].

Settings	**ABAQUS 2021**
Analysis Type	Steady state
Boundary Conditions	No constraints applied
Loads	Type: Pressure
Element Type	C3D10M (30373, 20-node quadratic hexahedral element)
Meshing Method	Manual (partitioning + seeding)
Approximate global Size	0.002

Table 6: Summary of some settings used for vibration Steady-State of 3D FEM of adhesive samples studied (ABAQUS software 2021).

The PZT KPEG 110 transducers have a significantly lower mass (m = 0.10 g) compared to the samples (e.g., for Sikadur 30, m = 3.71 g). As a result, their density, stiffness, and piezoelectric properties are neglected in

Journal Pre-proof

the 3D FEM model.

The optimized elastic properties (E_v, ν_v) of the adhesives were used to analyze their response to excitation over a frequency range of 300 points from 10 kHz to 250 kHz. The RUV spectra were plotted from a single nodal position at the center of the model in a spatial acceleration field. The experimental RUV spectra of the adhesives were then compared with the numerical spectra from the 3D steady-state dynamic finite element study to assess the resonance frequency measurement deviations.

3.6. Identification of the Viscoelastic Behavior

The viscoelastic behavior of the adhesives is explored by analyzing the ratio between the dynamic Young's modulus (measured via resonant ultrasonic vibration) and the static Young's modulus (obtained from tensile tests or literature). This ratio is studied as a function of the damping coefficient ζ, with the goal of identifying a mathematical relationship that characterizes the material response.

To this end, various functional forms, including linear and nonlinear (e.g., quadratic) models, are fitted to the experimental data using least-squares regression. The objective is to determine whether a consistent empirical law emerges across different adhesives that links stiffness and damping behavior. The resulting model, once validated, serves as a candidate for describing the viscoelastic response of the material.

Journal Pre-proof

Journal Pre-proof

4. Results

4.1. Densities of the various adhesive samples studied

The densities of the adhesive mixtures (resins and hardeners) were not provided in the technical data sheets for Sicomin SR5030, 3M Scotch-Weld 2216 B/A, and Sikadur 30. In contrast, density values were available for Loctite UK 1351 B25, SAF 30, and Araldite AV138M-1/HV998. The density values obtained experimentally using the OHAUS densitometer are reported in Table 7. The average measured values, along with the corresponding values from the manufacturers data sheets, are summarized in Fig.5. Notably, For the 3M2216 Scotch-Weld 2216 B/A adhesive, no indication of the density was provided in the data sheet.

Sample	**Density(kg/m^3)**	**Loctite**	**Saf 30**	**Sicomin**	**Araldite**	**3M2216**	**Sikadur 30**
1	ρ_1	1488.6	1148.4	1218.9	1584.7	1302.0	1867.0
2	ρ_2	1489.7	1149.4	1228.6	1610.4	1300.3	1862.2
3	ρ_3	1490.4	1146.4	1221.9	1611.0	1292.8	1877.3

Table 7: Measured densities of the six adhesives studied using the OHAUS densitomete.

Journal Pre-proof

Journal Pre-proof

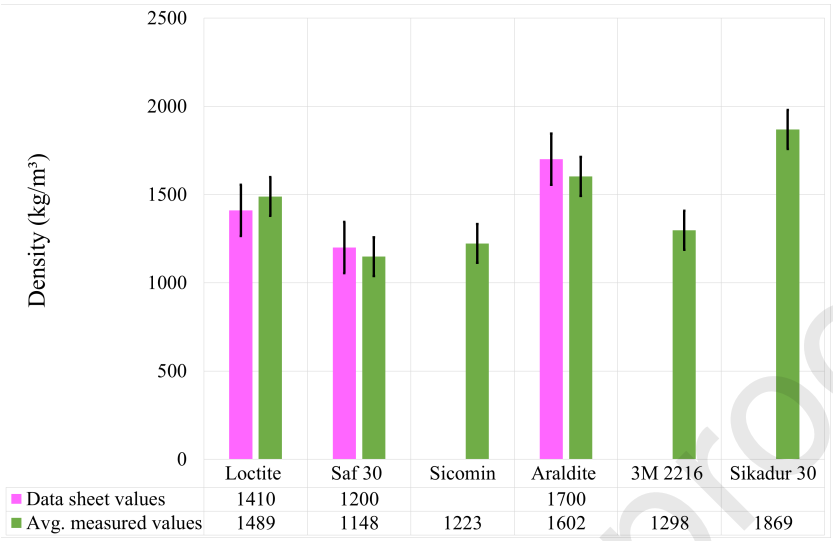

Figure 5: The average values for the measured densities of the six adhesives investigated, along with reference values reported in manufacturer datasheets.

4.2. Experimental measurements of the RUV spectra of the various adhesive samples studied

The various experimental RUV spectra of the adhesive samples measured are shown in Fig.11. From these measured experimental spectra, two resonance frequencies peaks (f^1_{exp}, f^2_{exp}) that coincide (are associated) with the first two natural compressional modes of the 3D numerical FEM of vibrational analysis allowing the identification of provisional Young's moduli and Poisson's ratios (E_p, ν_p) are grouped together in Fig. 6.

4.3. Vibrational Modal Analysis to identify mode shapes in experimental RUV spectra for the identification of Young's modulus and Poisson's ratios

A 3D numerical vibrational modal analysis was performed using the FEM in COMSOL Multiphysics [38] for six adhesives. The two selected natural

Journal Pre-proof

vibrational modes correspond to compressional shapes. Fig. 6 groups these first two longitudinal vibration mode values (f^1_{mode}, f^2_{mode}), enabling identification of provisional Young's moduli by fitting the theoretical curve to the experimental one, along with the provisional Poisson ratios (E_p, ν_p). For all six adhesives, these modes have the same shapes and correspond to the 9th and 32nd modes in the vibrational analysis (All 6 rigid body modes are taken into account), as shown in Fig.7.

Journal Pre-proof

Journal Pre-proof

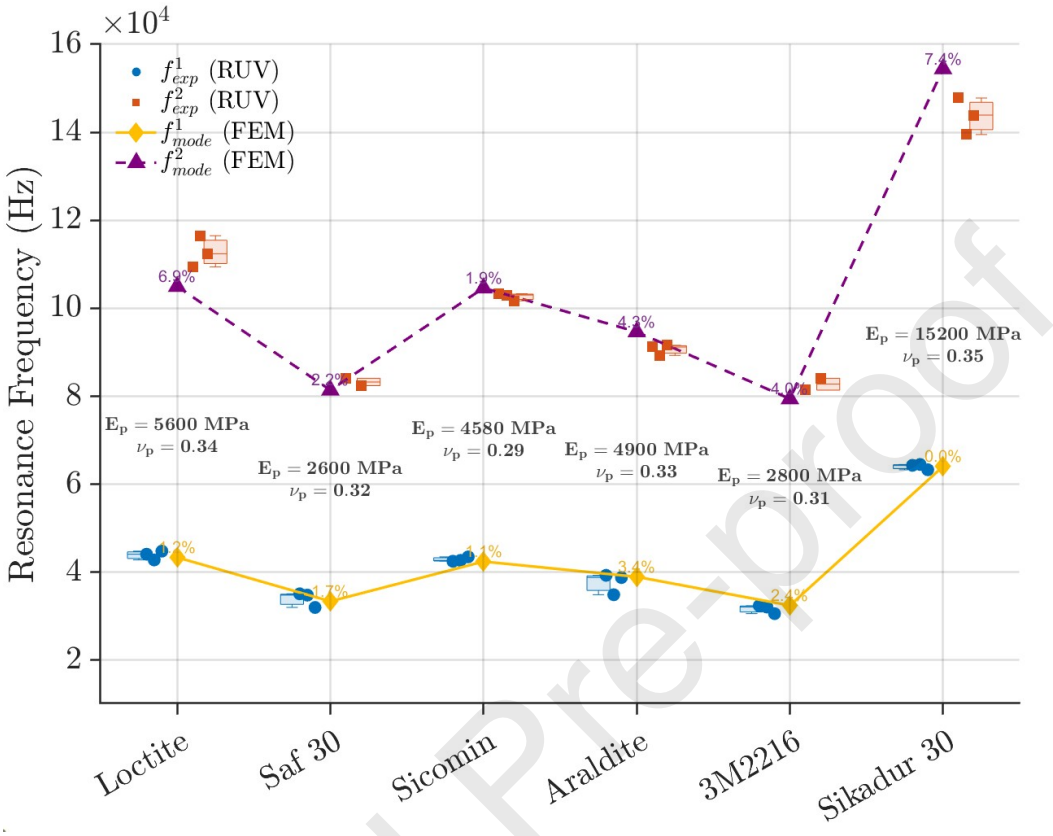

Figure 6: Comparison between the two experimental resonance peaks (RUV) and the first two compressional modes predicted by FEM for each adhesive (3 samples per adhesive). The relative errors between FEM and RUV modes are annotated, along with the provisional Young's moduli and Poisson's ratios used in the simulation.

.

Journal Pre-proof

Journal Pre-proof

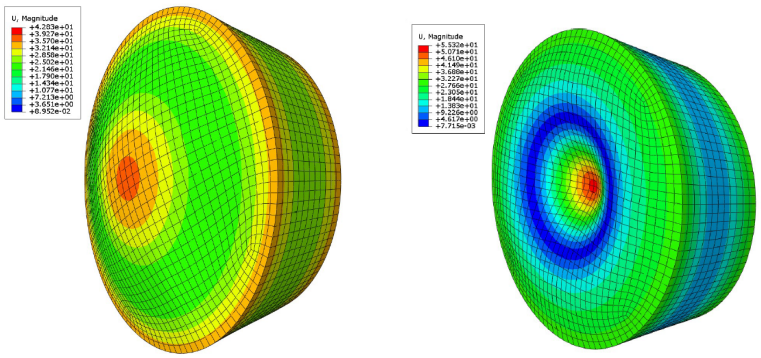

(a) First Longitudinal Mode Shape - Corresponds to the 9th Global Vibrational Mode.

(b) Mode Shape of the second Longitudinal Vibration, identified as the 32nd global mode in the system.

Figure 7: Natural vibration mode shapes of Adhesives with ABAQUS 2021 software.

4.4. Optimization of the values of Young's moduli and Poisson's ratios

4.4.1. Cost function

The cost function, used to recover the final (optimal) values of (E_v, ν_v), is calculated based on the two experimental resonance peaks listed in Fig. 6, the provisional elastic properties given in Fig. 6 (used as initial estimates), and the boundary constraints (upper and lower limits) defined in Table 8. The optimization results are illustrated through the scatter plots shown in Fig. 8.

Journal Pre-proof

Parameter	Loctite	Saf 30	Sicomin	Araldite	3M2216	Sikadur 30
lower boundary						
Lower Poisson ratio ν_L	0.29	0.29	0.29	0.29	0.29	0.29
Lower Young's Modulus E_L (MPa)	4000	400	4000	4000	400	10000
Upper boundary						
Upper Poisson ratio ν_U	0.4	0.4	0.4	0.4	0.4	0.4
Upper Young's Modulus E_U (MPa)	6000	3000	6000	6000	3000	16000

Table 8: Nelder Mead parameters for identifying the elastic properties of 6 adhesives studied

Journal Pre-proof

Journal Pre-proof

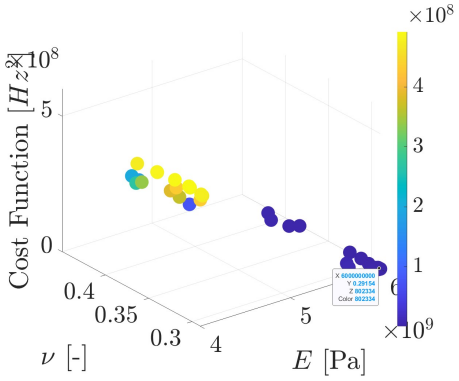

(a) Scatter plots of Loctite UK 1351 B25

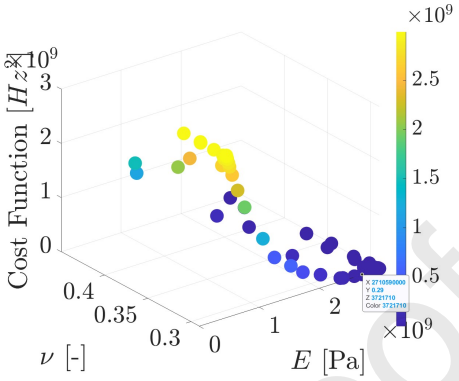

(b) Scatter plots of Saf 30 MIB

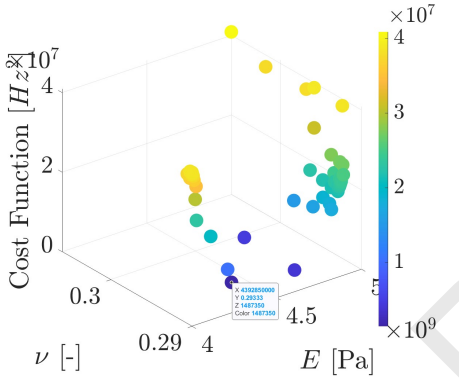

(c) Scatter plots of Sicomin SR5030

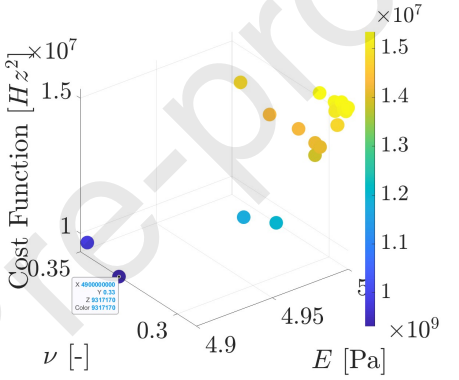

(d) Scatter plots of Araldite AV138M-1/HV998

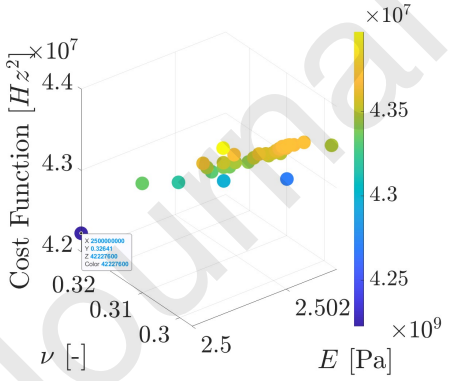

(e) Scatter plots of 3M2216 Scotch-Weld 2216 B/A

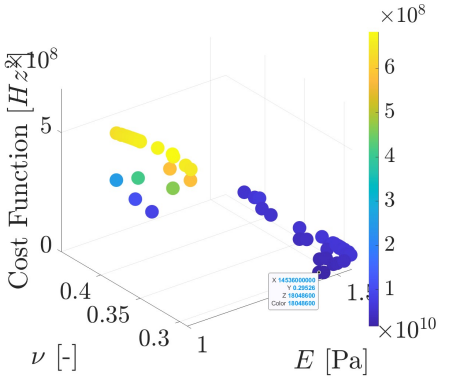

(f) Scatter plots of Sikadur 30

Figure 8: Optimisation of 6 adhesives studied with COMSOL Multiphysics 6.1 and MATLAB R2024a.

Journal Pre-proof

4.4.2. The final (optimal) elastic properties of the 6 studied adhesives

The technical datasheets of the adhesives studied provide static tensile Young's moduli, with the exception of 3M Scotch-Weld 2216 B/A. The final Young's moduli identified through vibration testing, along with literature values, are compiled in Fig.9. Specifically, K. Idrissa et al.[10] reported static tensile Young's moduli for Loctite UK 1351 B25 and Sikadur 30; R. J. C. Carbas et al.[19] provided the dynamic Young's modulus for Araldite AV138M-1/HV998; and T. Topkaya and M. Y. Solmaz[5, 6] reported the static tensile Young's modulus for 3M Scotch-Weld 2216 B/A. The Young's moduli of SAF 30 and 3M Scotch-Weld 2216 are low because their glass transition temperatures are around 30 °C, which are lower than those of the other adhesives. However, when looking at the dynamic Young's moduli, it appears that the glass transition temperature is not the only factor influencing the mechanical behavior. In this case, the Tg mainly affects SAF 30 and 3M Scotch-Weld 2216, while the adhesives with Tg values above 50 °C exhibit similar Young's moduli. This suggests that, beyond a certain Tg threshold, other factors such as crosslinking density, formulation, and filler content may play a more dominant role in determining the mechanical properties.

In contrast, Poisson's ratios are generally not reported in the technical datasheets nor in the literature, with the exceptions of Sikadur 30 (M. Lamberti et al.[13], using static tensile tests) and 3M Scotch-Weld 2216 B/A (T. Topkaya and M. Y. Solmaz[5, 6], also using static tensile tests). The different values of the Poisson's ratios identified for the adhesives studied are summarized in Fig. 10.

Journal Pre-proof

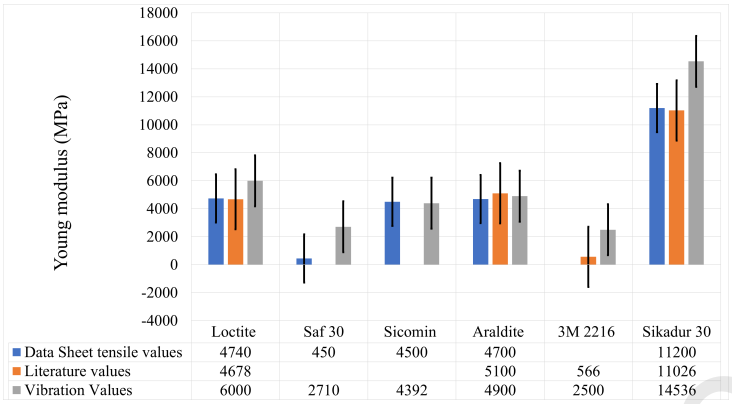

Figure 9: Young's moduli of 6 adhesives studied (with Error bars).

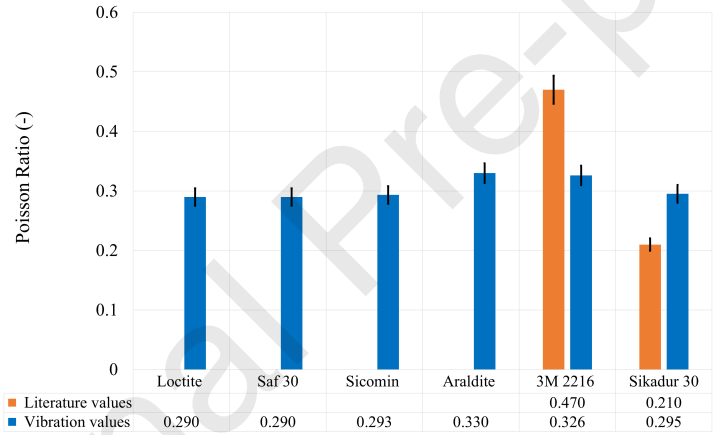

Figure 10: Poisson's ratios of the 6 adhesives studied. The literatue values are from [5, 6, 13]

4.4.3. Determination of Glass transition (T_g) of various adhesives studied

To better interpret the low Young's modulus values obtained from Resonant Ultrasound Vibrations (RUV)—particularly for the adhesives with the lowest stiffness—it was necessary to determine their glass transition temperatures (T_g). Since the data sheets provided incomplete information on T_g

Journal Pre-proof

(see Table 9), differential scanning calorimetry (DSC) measurements were performed. The analyses were carried out using a ChipDSC 10 instrument (Mettler Toledo, Switzerland) at the IUSTI Laboratory in Marseille, France. Disk-shaped samples (4 mm in diameter and 2 mm thick) were tested under ambient conditions (room temperature and atmospheric pressure). The measured T_g values are summarized in Table 9.

	Loctite	**Saf 30**	**Sicomin**	**Araldite**	**3M2216**	**Sikadur 30**
Curing schedules before demolding at 23°C (Days)	1	1	1	1	1	1
Curing Time at 23°C (Days)	12	11	12	13	12	13
Age distribution from demolding to testing (Days)	12	11	12	13	12	13
Measured Glass transition values T_g (°C)	59	-	60	58	-	57

The glass transition temperature (T_g) below 30 °C could not be determined (-).

Table 9: Glass transition temperatures T_g of the studied adhesives.

Detecting the T_g was challenging for two samples. They could not be determined for the 3M 2216 and SAF 30 adhesives due to the limited sensitivity of the instrument, which could not detect T_g values below 30 °C (considered the lowest).

4.5. Confrontation of experimental RUV spectra with 3D Numerical FEM (Steady-State) spectra of 6 adhesives

These two optimized elastic parameters were used in the 3D numerical (FEM) whose spectra were compared with the experimental spectra as illustrated in Fig.11. The 3D numerical RUV spectra of adhesives were named respectively LC-S, SF-S, SC-S, AR-S, 3M-S and SK-S.

Journal Pre-proof

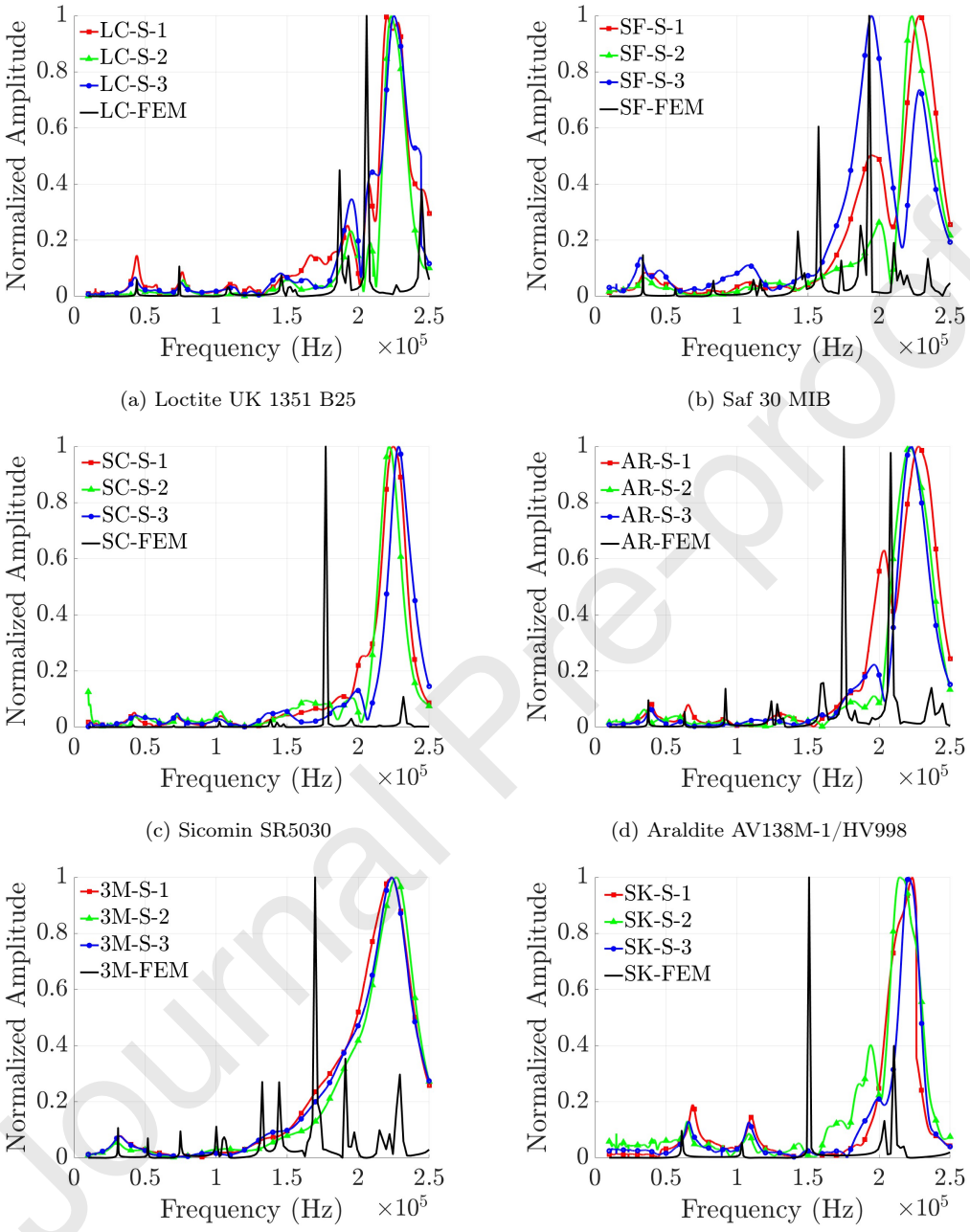

(a) Loctite UK 1351 B25

(b) Saf 30 MIB

(c) Sicomin SR5030

(d) Araldite AV138M-1/HV998

(e) 3M2216 Scotch-Weld 2216 B/A

(f) Sikadur 30

Figure 11: Confrontation of experimental ultrasonic vibration Spectra from PZT and Numerical 3D steady state simulations (1: First mode, 2: Second mode and H: High resonance peak).

Journal Pre-proof

4.6. *Identification of the Viscoelastic Behavior of the studied adhesives: Young modulus ratio and damping coefficients*

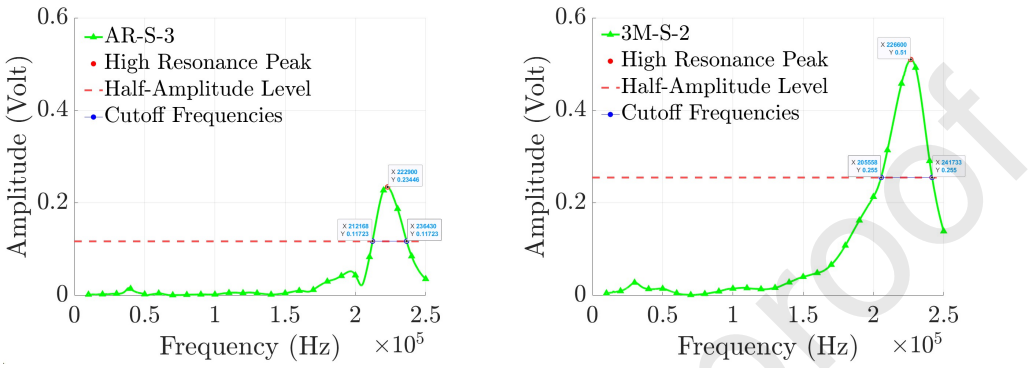

(a) Araldite (b) 3M2216

Figure 12: High resonance peak frequencies $f_{\max}^{\exp}$ and mid-amplitude widths Δf corresponding to experimental resonant ultrasonic vibration spectra. The amplitude represents the PZT responses in Volt

To analyze the behavior of 6 adhesives studied, the ratios R_E between the Young's moduli recovered from the RUV tests and those obtained in static tensile tests from the literature or the data sheets of these different adhesives were calculated using Eq. 5. In addition, the damping coefficients were also calculated using the Eq. 6 (see Fig.12). The values of the ratios R_E and the damping coefficients ζ are grouped in Table 10 and the regression curve of the Young's modulus ratios of the set of adhesives as a function of the damping coefficient is illustrated in Fig. 13.

Journal Pre-proof

Adhesives	**Loctite**	**Saf 30**	**Sicomin**	**Araldite**	**3M2216**	**Sikadur 30**
			Resonance frequencies (Hz)			
$f_{\max}^{\exp}$	225200	228500	228300	222900	226600	214700
ζ	0.061	0.057	0.041	0.054	0.079	0.056
R_E	1.265	4.517	0.976	1.042	4.416	1.297

Table 10: Young's Modulus Ratios and Damping coefficient of 6 adhesives studied.

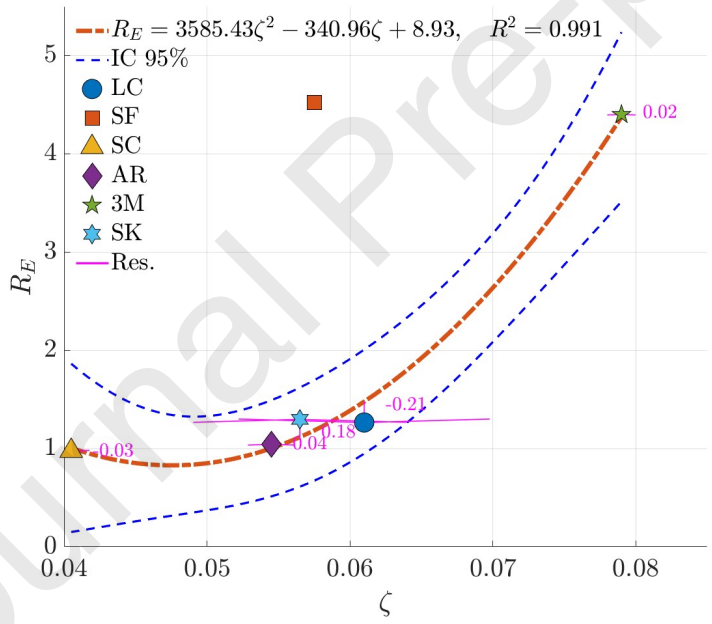

Figure 13: Quadratic fit with confidence interval and residuals of the Young's modulus ratios of the set of adhesives as a function of the damping factor (The names of adhesive are abbreviated; LC: Loctite, SF: Saf 30, SC: Sicomin, AR: Araldite, 3M: 3M2216 and SK: Sikadur 30).

Journal Pre-proof

Based on the curve fitting in Fig. 13, which expresses a quadratic relationship between the ratio of Young's moduli and the damping coefficient of the various structural adhesives studied, as well as all the considerations discussed in Section 5.5 regarding the validation of the model as demonstrated by Eq. 17. The results highlight how adhesives can be selected based on the stiffness–damping trade-off across different industries. In the automotive sector, low-stiffness, high-damping adhesives are favored to improve vibrational and acoustic comfort, particularly for bonding body panels such as hoods and doors. In contrast, aerospace applications demand highly rigid adhesives to ensure efficient load transfer in composite components like spars, ribs, and panels. The marine sector requires a balance between stiffness and damping to withstand structural loads while mitigating vibrations from waves and engines; for example, moderately stiff adhesives are often used in interior panels to enhance passenger comfort. Investigating adhesive behavior at frequencies relevant to fastener resonance (50–500 kHz) provides valuable insight into their potential role in hybrid joining and load-sharing configurations across sectors such as aerospace, automotive, and wind energy.

4.7. Validation of the Young's modulus and Poisson's ratios obtained using RUV tests via the impulse tests

The experimental FFT spectra of the temporal responses to rectangular pulses (width 15 μs) are shown in Figs. 14a - 14f.

Journal Pre-proof

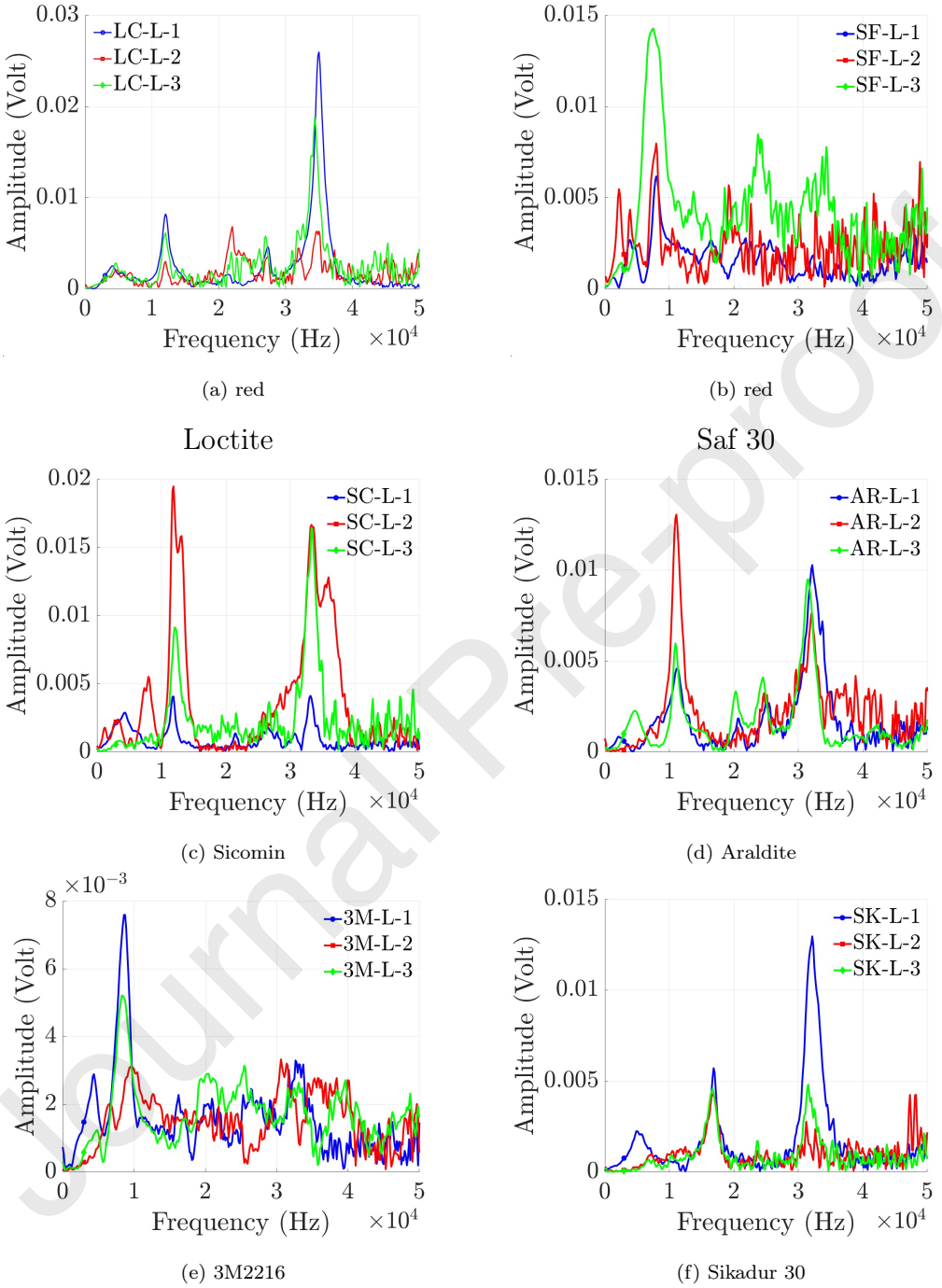

(a) red

(b) red

(c) Sicomin

(d) Araldite

(e) 3M2216

(f) Sikadur 30

Figure 14: FFT spectra of various adhesives from Laser vibrometer.

Journal Pre-proof

Based on the FFT curves of the Figs. 14a - 14f. In particular, all the first two compressive vibrational modes of the FEM of the different larger adhesives coincide with the corresponding resonance frequencies of their FFT spectra, as shown in Fig. 15. The relative error (D^1_{mode} and D^2_{mode}) between the maximum values of the first two compressive vibrational modes of the FFT (see Fig 15) and the FEM (see Fig 15) for studied adhesives is shown in Table 11.

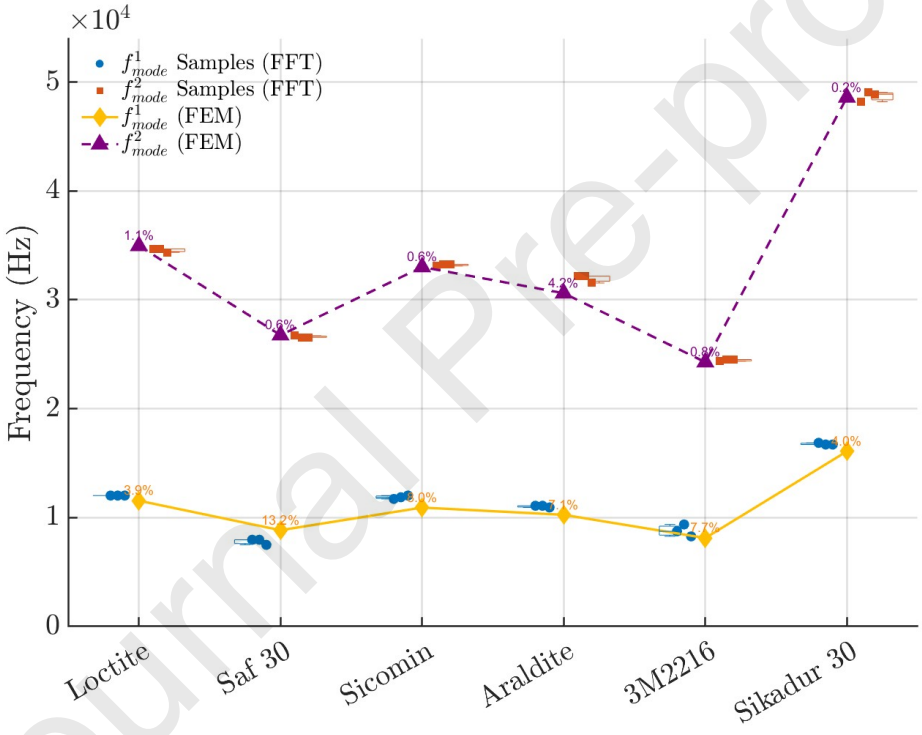

Figure 15: First two resonance peaks (f^1_{mode} and f^2_{mode}) of larger adhesive samples: comparison between FFT measurements and 3D FEM simulations (compressive vibrational modes), with relative errors indicated.(three samples per adhesive type).

Journal Pre-proof

Relative error	Loctite	Saf 30	Sicomin	Araldite	3M2216	Sikadur 30
D^1_{mode} (%)	3.9	13.2	8.0	7.1	7.7	4.0
D^2_{mode} (%)	1.15	0.6	0.6	4.2	0.8	0.2

Table 11: The relative errors between FEM and FFT-measured of the studied adhesives.

4.8. The synthesis and statistical analysis (ANOVA and Kruskal-Wallis tests) of mechanical properties of various adhesives.

The synthesis of the mechanical properties of the studied adhesives are summarized in Table 12.

Parameter	Loctite	Saf 30	Sicomin	Araldite	3M2216	Sikadur 30
Static properties from data sheet or literature						
Poisson ratio ν_s	-	-	-	-	0.47 [5]	0.21 [13]
Young's modulus E_s (MPa)	4740*, 4678 [10]	400*-600*	4500*	4700*	566 [5]	11200*, 11026 [10]
Vibration (Dynamic) properties from current study						
Poisson ratio ν_v	0.29	0.29	0.2933	0.33	0.326	0.295
Young's modulus E_v (MPa)	6000	2710	4392	4900	2500	14536
Damping coefficient ζ	0.061	0.057	0.041	0.054	0.079	0.056
Young modulus ratio R_E	1.265	4.517	0.976	1.042	4.416	1.297

Data sheet values (*).

No indicated values in data sheet (-).

Table 12: Synthesis of the static and dynamic properties of the studied adhesives.

ANOVA or Kruskal-Wallis tests require multiple observations per group. Since the mechanical properties were measured collectively for the three sam-

Journal Pre-proof

ples rather than individually, these tests could not be performed. Nevertheless, an exploratory approach simulated a ±5% variability (n=5 per type of adhesive) to illustrate the potential statistical differences between the adhesives. The results of the statistical tests (ANOVA and Kruskal-Wallis tests) are shown in Fig. 16.

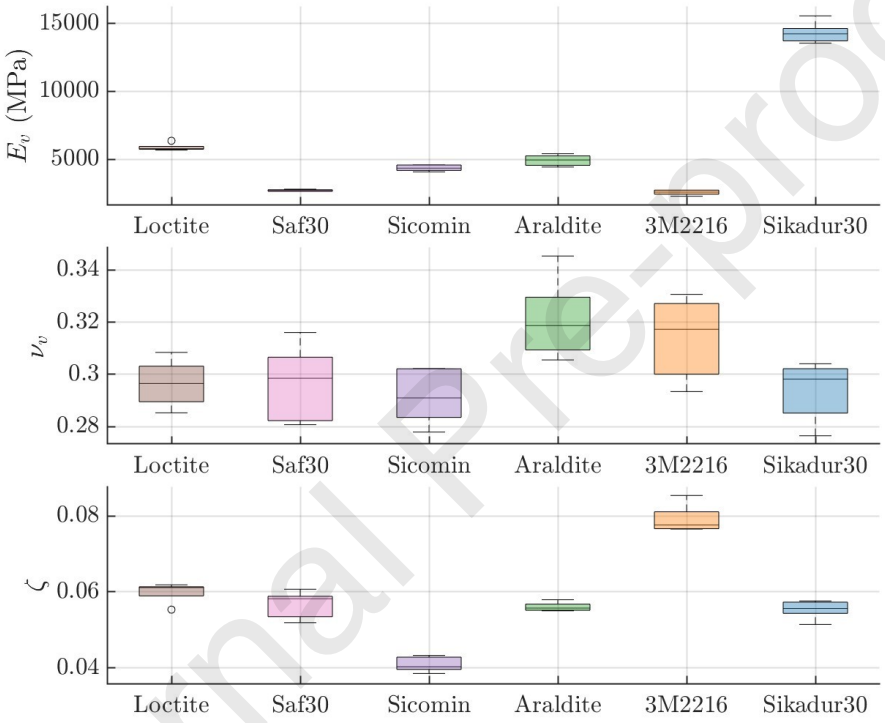

Figure 16: Statistical analysis (ANOVA and Kruskal-Wallis tests) of mechanical properties of various adhesives studied

.

Journal Pre-proof

5. Discussions

5.1. Measured densities of 6 adhesives

The density values of the six adhesives measured using the densitometer, as presented in Fig.5, show a dispersion of the measurements of about 2%. Comparing these measured values with those in the data sheets (see Fig.5), small deviations of around 5% were observed. These may be due to the lack of effective control of porosity (presence of voids and air bubbles) during the manufacturing process (preparation of the mixes) of the adhesive samples. In fact, these deviations are acceptable. Sikadur 30 is the densest, followed by Araldite AV138/HV998, Loctite UK 1351 B25, 3M2216 Scotch-Weld 2216 B/A, Sicomin SR5030 and finally Saf 30 MIB.

Since there is no specific standard for controlling the porosity of adhesives or determining their void percentage, some authors have attempted to measure it [13, 42, 43, 44], while others have sought to reduce it using ultrasonic vibration methods [45]. These methods mainly focus on the volume of pores on the external surface, as reported by the authors in reference [42]. Since the volume of internal pores in the adhesives does not communicate with the peripheral pores (see Fig. 17), these internal pores are not taken into account in the density estimation.

Journal Pre-proof

Journal Pre-proof

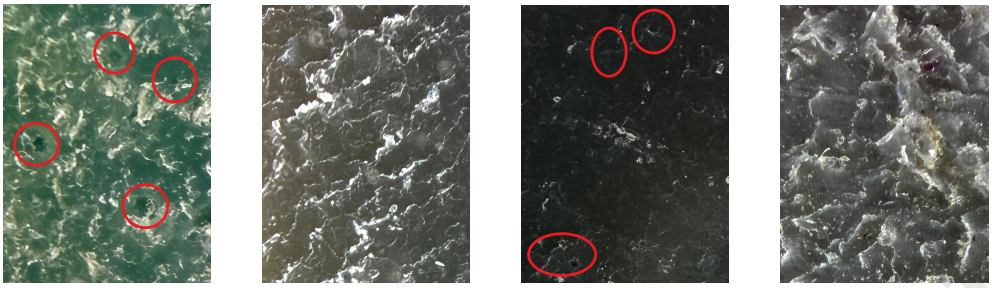

(a) (b) (c) (d)

Figure 17: Microstructures of selected prepared adhesive samples. The image corresponds to a field of view of approximately 1.5 mm × 1.1 mm, with an estimated spatial resolution of 1.46 μm/pixel using an APEXEL 200X Phone Microscope Lens (Shenzhen, Guangdong, China) combined with an Apple IPhone 16E (Cupertino, CA 95014 United States) - X10 magnification

(a) Loctite; (b) Araldite; (c) 3M2216; (d) Sikadur 30.

Lamberti et al. [13] estimated the porosity of the Sikadur 30 adhesive to be approximately 5%. AlZubi et al. [42] reported a porosity of around 2% for the same adhesive, where the porosity percentage was evaluated based on the external surface area of the samples.

To validate the density values, we fabricated additional cubic samples with a volume of 7 mm^3, using the same manufacturing process as for the previously tested disk-shaped samples (see Fig. 2). Their densities were then measured using two methods: first with the OHAUS densitometer balance (Nänikon, Switzerland), as for the disk samples (see Fig. 2), and then using a helium pycnometer (Accupyc II 1340, Micromeritics Instrument Corporation, USA) equipped with a 1 cm^3 cell (diameter: 1.15 cm, height: 1.1 cm), in accordance with ASTM D4892-24 standard [46], for more accurate measurements, particularly in the presence of closed porosity. This technique uses

Journal Pre-proof

helium's ability to penetrate nanometric pores to measure volume by gas displacement. The helium pycnometer performs 10 volume measurements per sample to calculate an average density. The dispersion of the density measurements was 4%. All results are presented in Fig. 18. The consistency of the values obtained using two methods and samples with varying geometries validates the measured density values of the different adhesives studied.

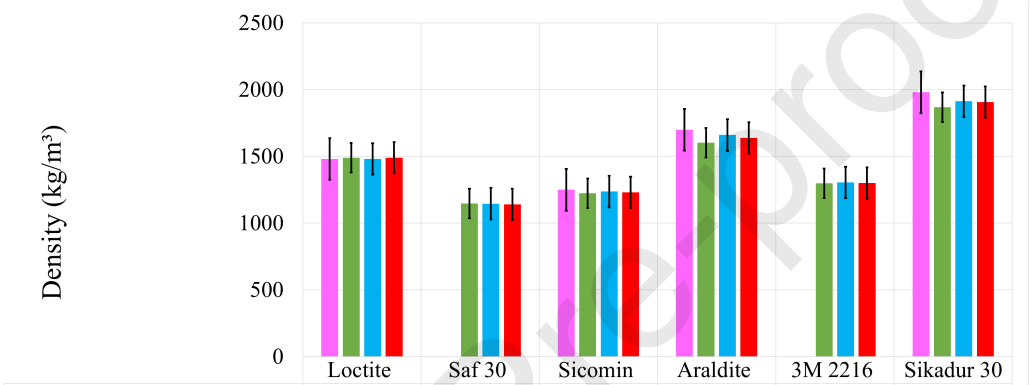

	Loctite	Saf 30	Sicomin	Araldite	3M 2216	Sikadur 30
Data sheet values	1480		1250	1700		1980
Disk samples (Densitometer)	1489	1148	1223	1602	1298	1869
Cubic samples (Pycnometer)	1481	1146	1237	1660	1305	1913
Cubic samples (Densitometer)	1489	1141	1230	1639	1300	1906

Figure 18: Validation of the density values of the disk-shaped samples (see Fig. 5) using small cubic samples and two measurement techniques: a densitometer and a helium pycnometer.

5.2. Young's modulus and Poisson ratios of 6 adhesives

- Regarding Young's modulus E_v: The results presented in Fig. 9 show that, for five of the six adhesives studied, the Young's modulus values obtained from vibration tests are higher than those measured in static tension (datasheets and literature). These adhesives are Loctite UK 1351 B25, Saf 30 MIB, Araldite AV138/HV998, 3M Scotch-Weld 2216 B/A, and Sikadur 30.

Journal Pre-proof

In contrast, Sicomin SR5030 shows a Young's modulus in vibration of the same order as in static tension.

The stiffness, ranking based on vibration tests, is as follows: Sikadur 30 is the stiffest, followed by Loctite UK 1351 B25, Araldite AV138/HV998, Sicomin SR5030, Saf 30 MIB, and finally 3M Scotch-Weld 2216 B/A.

- Regarding Poisson ratios ν_v: The results shown in Fig. 10 indicate that Araldite AV138/HV998 is the most flexible based on vibration tests, followed by 3M Scotch-Weld 2216 B/A, Sikadur 30, Sicomin SR5030, Saf 30 MIB, and Loctite UK 1351 B25.

  Poisson's ratio values for these adhesives are generally absent from technical datasheets and the literature, except for Sikadur 30 and 3M Scotch-Weld 2216 B/A. For Sikadur 30, M. Lamberti et al. [13] reported a static Poisson ratio ($\nu_s = 0.21$) lower than the value obtained from vibration tests ($\nu_v = 0.29$). Conversely, for 3M Scotch-Weld 2216 B/A, T. Topkaya and M. Y. Solmaz [5, 6] reported a static Poisson's ratio ($\nu_s = 0.47$) higher than the vibrational value ($\nu_v = 0.3264$).

5.3. Experimental and Numerical RUV spectra of 6 adhesives studied

The coincidence of the RUV spectra (experimental and 3D numerical) as shown in Fig.11 is a major indicator that the elastic properties (Young's moduli and Poisson's ratios) of the 6 adhesives studied are acceptable despite the small deviations observed. Some peaks in the experimental spectra are barely visible compared to the peaks in the 3D numerical FEM spectra. Given that the resonance frequencies of adhesives are directly related to their elastic properties, these peak shifts can be caused by the following : On one side,

Journal Pre-proof

observed errors of approximately 2% in the density measurements, possibly caused by a lack of understanding of the porosity (void distribution or the presence of air) within the different excited samples. Table 2 indicates that a 0.1% error in the mass measurement can lead to an error of approximately 0.1% in the Young's modulus value (indirectly on the frequencies).

A dimensional tolerance of 0.2 mm was observed in the mold fabrication for both diameter and thickness. This corresponds to relative errors of 0.6% and 0.8%, respectively, in the calculated values of Young's modulus, as summarized in Table 2.

It should be noted that the RUV spectra of the three samples of each adhesive type (see Fig. 11) were very similar, that means, they had the same geometry and boundary conditions (The attachment of the exciter and sensor to the samples were identical). The frequency deviations between RUV and FEM spectra are show in Fig. 19.

Journal Pre-proof

Journal Pre-proof

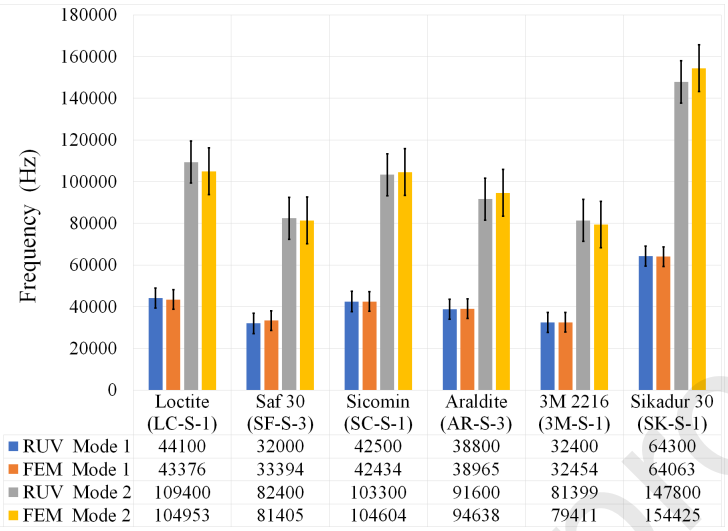

Figure 19: Frequency deviations in the comparison between the RUV and FEM spectra of the different adhesives (Modes 1 and 2).

5.4. Modulus Ratio and Damping Coefficient of Six Adhesives

Based on the damping ratios and Young's modulus ratios presented in Table 10, and the corresponding fitted curve of ζ versus R_E shown in Fig. 13, which exhibits a quadratic trend, the following observations can be made:

- Regarding Modulus ratio R_E, according to Eq.5, Saf 30 MIB, 3M2216, Sikadur 30, Araldite, and Loctite adhesives exhibit viscoelastic behavior ($R_E > 1$). In contrast, Sicomin adhesives ($R_E \approx 1$) behave elastically, with low energy dissipation, an instantaneous response, and a stable microstructure. They are minimally affected by strain rate and maintain consistent performance regardless of viscoelastic or microstructural effects.

- Regarding damping ζ, analysis of the two resonant frequencies from the experimental resonant ultrasonic vibration spectra of the six adhesives,

Journal Pre-proof

as shown in Fig. 6 and Fig. 11, reveals that the first two associated compressional mode shapes have the same ranking. These modes occur within the same frequency range, between 10 kHz and 150 kHz, and are characterized by small amplitude variations.

However, adhesives do not exhibit identical natural frequencies, they do have the same mode shapes, as illustrated in Fig. 7. Within this frequency range, all six adhesives show a weak response to ultrasonic vibration excitations.

A second frequency range, located above 150 kHz, was identified for all six adhesives. It is characterized by large amplitude variations in their respective vibration response spectra, indicating high sensitivity to ultrasonic vibration excitations. Consequently, this regime (range) was studied in greater detail. Damping coefficients were calculated based on the frequencies corresponding to the maximum amplitude in the spectrum of each adhesive.

The vibration modes obtained by the 3D FEM, associated with these maximum amplitude frequencies, were found to exhibit different modal ranks and shapes in the adhesives, except for Loctite UK 1351 B25 and Sicomin SR5030, which showed similar modal behavior (see Fig. 20).

However, 3M Scotch-Weld 2216 B/A exhibited the highest damping coefficient ζ among adhesives, indicating superior vibration damping capacity, followed by Loctite UK 1351 B25, Saf 30 MIB, Sikadur 30, Araldite AV138M-1/HV998, and finally Sicomin SR5030 (see Table. 10).

Journal Pre-proof

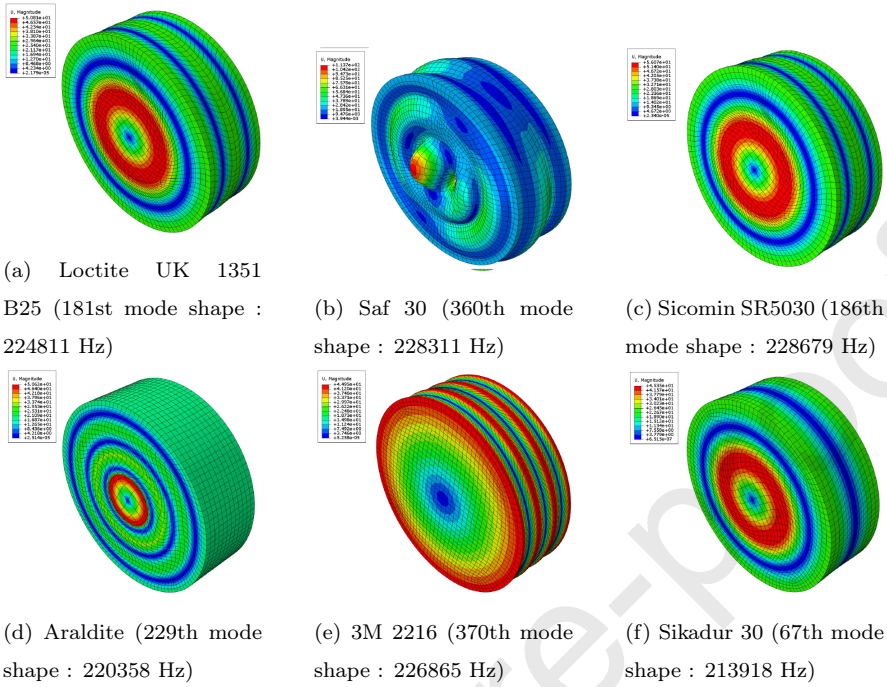

(a) Loctite UK 1351 B25 (181st mode shape : 224811 Hz)

(b) Saf 30 (360th mode shape : 228311 Hz)

(c) Sicomin SR5030 (186th mode shape : 228679 Hz)

(d) Araldite (229th mode shape : 220358 Hz)

(e) 3M 2216 (370th mode shape : 226865 Hz)

(f) Sikadur 30 (67th mode shape : 213918 Hz)

Figure 20: 3D FEM mode shapes (computed using ABAQUS software 2021) corresponding to the high-frequency resonance peaks observed in the experimental RUV spectra.

Visually, the experimental peaks appear as well-centered bell shapes, indicating a high degree of symmetry and suggesting minimal modal coupling or noise interference (see Fig 20). The symmetry of the spectral peaks for the different adhesives-on which the damping values were computed-is clearly confirmed. This is quantitatively assessed by comparing the half-widths at half-maximum on either side of the experimental peak frequency $f_{\max}^{\exp}$:

$$\Delta f_1 = f_{\max}^{\exp} - f_1, \quad \Delta f_2 = f_2 - f_{\max}^{\exp}$$

where f_1 and f_2 are the cutoff frequencies, i.e., the frequencies at which the amplitude drops to half of the peak value). A peak is considered symmetric

Journal Pre-proof

if:

$$|\Delta f_1 - \Delta f_2| \leq 0.1 \cdot f_{\max}^{\exp} \tag{9}$$

Fig. 21 validates the half-power bandwidth method for damping estimation (see Eq. 9). The peaks show near-Lorentzian profiles, confirming the method's reliability.

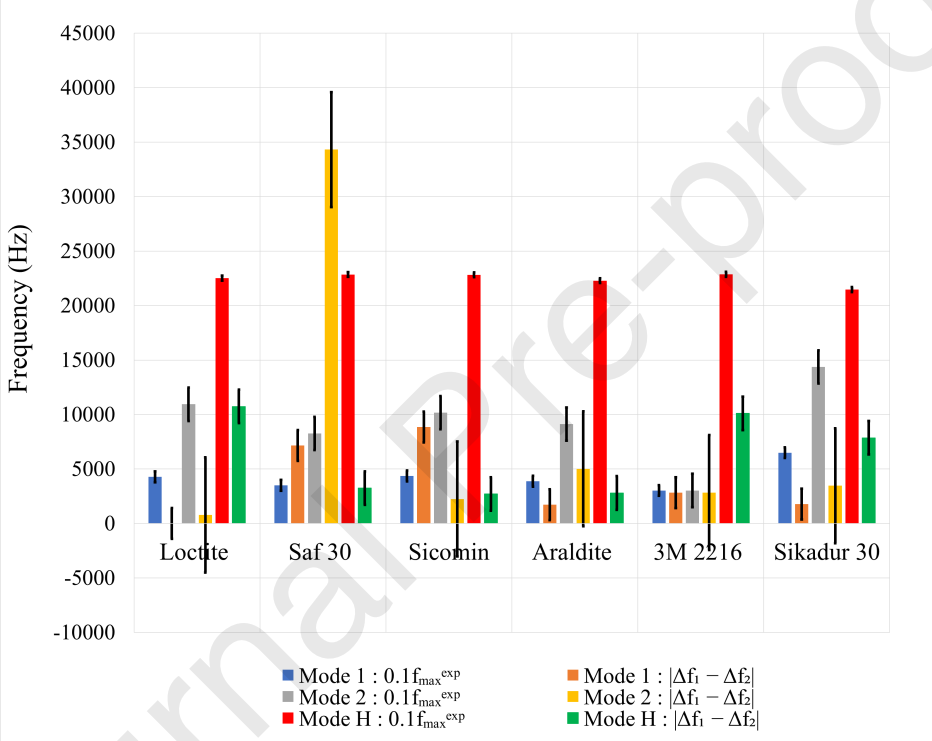

Figure 21: Damping symetric validation of various adhesives studied (H: High resonance peak H corresponds to the mode shape shown in Fig. 20)

.

The values in Fig. 22 show that the low-damping assumption ($\zeta < 0.1$), essential for the half-power bandwidth method. It is satisfied for a high-frequency bandwidth (> 200 kHz). For $\zeta \leq 0.08$, deviations are negligible

Journal Pre-proof

($< 2\%$), validating the method. At $\zeta \approx 0.1$, a slight loss of accuracy appears, without affecting the central frequency. Beyond this, the method becomes less reliable: the bandwidth is overestimated and peaks are distorted.

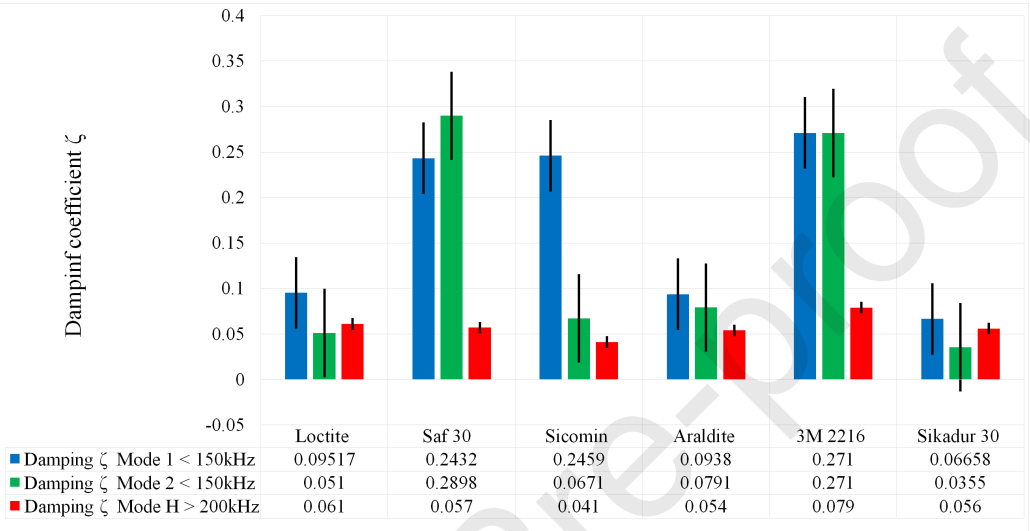

	Loctite	Saf 30	Sicomin	Araldite	3M 2216	Sikadur 30
Damping ζ Mode 1 < 150kHz	0.09517	0.2432	0.2459	0.0938	0.271	0.06658
Damping ζ Mode 2 < 150kHz	0.051	0.2898	0.0671	0.0791	0.271	0.0355
Damping ζ Mode H > 200kHz	0.061	0.057	0.041	0.054	0.079	0.056

Figure 22: Damping coefficient of various adhesives studied (Mode 1 and Mode 2 correspond respectively to the first two compressional modes; Mode H corresponds to the mode shape shown in Fig. 20.)

5.5. Justification of the Quadratic Fit

This section provides a theoretical justification for the quadratic relationship observed between the damping ratio ζ and the modulus ratio R_E, grounded in viscoelastic theory and supported by experimental fitting results.

A quadratic fit provided the best agreement with the experimental data that relate the damping coefficient ζ to the modulus ratio R_E, as shown in Fig. 13.

Journal Pre-proof

5.5.1. General Storage Modulus Expression

For a damped material, the **complex modulus** in the Kelvin-Voigt model (consists of a spring and dash-pot in parallel) is given by [47]:

$$E^* = E' + \mathrm{i}\eta\omega \tag{10}$$

where:

- E' represents the storage modulus,
- $\eta\omega$ is the loss modulus,
- η is the viscosity coefficient,
- ω is the angular frequency.

5.5.2. Loss Tangent

The loss tangent is defined as:

$$\tan\delta = \frac{\eta\omega}{E'}, \tag{11}$$

where δ is the phase angle between stress and strain.

For small damping, the **damping coefficient** is:

$$\zeta \approx \tan\delta \tag{12}$$

The Kelvin-Voigt model naturally leads to a quadratic dependence of storage modulus on damping due to the relationship between damping and viscosity;

$$E' = E_0 + k\zeta^2, \tag{13}$$

where k is a proportionality constant.

Journal Pre-proof

Journal Pre-proof

For general damping, we assume the storage modulus depends on the damping coefficient ζ:

$$E'(\zeta) = E_0 + f(\zeta) \tag{14}$$

where $f(\zeta)$ is a smooth function.

5.5.3. Maclaurin Expansion of the Storage Modulus

Expanding $f(\zeta)$ in a **Maclaurin series** around $\zeta = 0$:

$$E'(\zeta) = E_0 + k_1\zeta + k_2\zeta^2 + O(\zeta^3) \tag{15}$$

where:

- $k_1 = f'(0)$ represents the **linear dependence on damping**. The linear term $a_1\zeta$ arises from first-order effects of damping, which may depend on material-specific behavior.
- $k_2 = \frac{1}{2}f''(0)$ represents the **quadratic dependence on damping**. The quadratic term $a_2\zeta^2$ corresponds to higher-order effects, which become dominant as damping increases.

This means that:

1. **For small damping**, the storage modulus **changes linearly** with damping.
2. **For moderate damping**, the storage modulus follows a **quadratic dependence**.

Eq.15 for **general damping**, is **consistent with our experimental results**, see Fig.13 showing a mix of linear and quadratic dependence of E' on damping. It is more **general** than the purely quadratic fit, and olso aligns with **experimental observations** in viscoelastic materials and adhesives.

Journal Pre-proof

5.5.4. Incorporating the Doi-Edwards Model [48]

For entangled polymers, the Doi-Edwards model provides relationship between the intrinsic and the static modulus:

$$E_0 \approx k_0 E_{\text{static}}, \tag{16}$$

where:

- k_0 is a constant given in Appendix A,
- It is function of L_e, the entanglement length and l_p, the persistence length.

Using this relationship and knowing that $E_0 \gg E_{\text{static}}$, we express the storage modulus in terms of the entanglement (plateau) modulus:

$$E' = E_{\text{dynamic}} = E_{\text{vibration}} = k_0 E_{\text{static}} + k_1 \zeta + k_2 \zeta^2. \tag{17}$$

This equation demonstrates how the entanglement effects contribute to the elastic response, while the damping effects introduce a quadratic dependence. The normalized dynamic modulus ratio R_E is:

$$R_E = e_0 + e_1 \zeta + e_2 \zeta^2, \tag{18}$$

$$\text{where} \quad e_0 = k_0, \quad e_1 = \frac{k_1}{E_{\text{static}}} \quad \text{and} \quad e_2 = \frac{k_2}{E_{\text{static}}}.$$

5.5.5. The physical meaning of the parameters and their relationship with the microstructure of the material (such as crosslinking degree and chain entanglement)

Starting from the quadratic relation in Eq. 18 between the Young's modulus ratio and the damping coefficient, the quadratic fit effectively models

Journal Pre-proof

the nonlinear viscoelastic behavior of adhesives by linking macroscopic parameters (E_v, ζ) to microstructural features (L_e, l_p). This provides a physical framework for interpreting the observed viscoelastic responses. A high quadratic coefficient(e_2), reflects a high degree of crosslinking or significant entanglement of polymer chains [48, 49], thereby influencing the overall mechanical response.

It is important to note that the Doi–Edwards theory serves as a conceptual framework for interpreting relaxation in entanglement-dominated polymers, rather than as a universal model.

The curve shown in Fig. 23 was generated from the fitted equation.

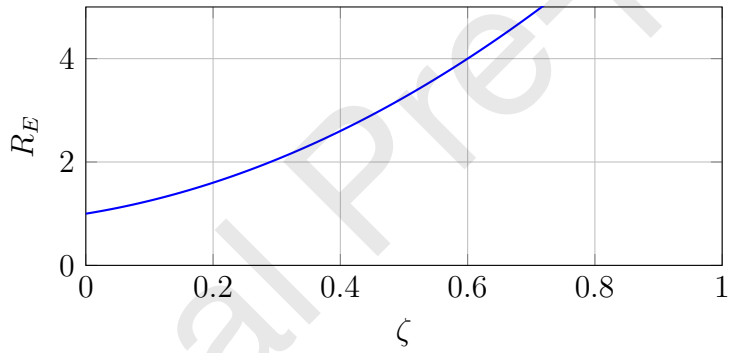

Figure 23: Evolution of R_E as a function of ζ for $e_2 = 3585.43$, $e_1 = -340.96$, and $e_0 = 8.93$.

This plot shows that for low damping, the modulus ratio remains close to 1. As ζ increases, R_E initially rises almost linearly, then more sharply due to the influence of the quadratic term.

Journal Pre-proof

5.5.6. Comparative Analysis of Quadratic and Linear-Quadratic Models using AIC/BIC

Based on the behavior law of the adhesives studied in Fig. 13, we have:

- Quadratic model:

$$R_E = 3585.43 \cdot \zeta^2 + 8.93 \tag{19}$$

- Linear-quadratic model:

$$R_E = 3585.43 \cdot \zeta^2 - 340.96 \cdot \zeta + 8.93 \tag{20}$$

These two models are compared using the AIC (Akaike Information Criterion) and BIC (Bayesian Information Criterion), which assess both the goodness of fit and the model complexity:

$$\mathrm{AIC} = 2k + n \cdot \ln\left(\frac{\mathrm{SSE}}{n}\right), \quad \mathrm{BIC} = k \cdot \ln(n) + n \cdot \ln\left(\frac{\mathrm{SSE}}{n}\right)$$

where: $n = 6$ is the number of data (adhesive studied) points, k is the number of model parameters ($k = 2$ for quadratic model and $k = 3$ for linear-quadratic model), and SSE is the sum of squared residuals:

$$\mathrm{SSE} = \sum_{i=1}^{n} \left(R_{E_i} - \hat{R}_{E_i}\right)^2$$

The comparison between quadratic and linear-quadratic model predictions and their squared errors is shown in Table 13, and the information criteria (AIC / BIC) are presented in Fig. 24.

Journal Pre-proof

ζ	R_E	$\hat{R}_E^{\text{quad}}$	$(R_E - \hat{R}_E)^2_{\text{quad}}$	$\hat{R}_E^{\text{lin-quad}}$	$(R_E - \hat{R}_E)^2_{\text{lin-quad}}$
0.061	1.265	13.34	146.3	1.47	0.042
0.057	4.517	20.53	256.8	1.15	11.3
0.041	0.976	14.95	193.7	0.98	0.0004
0.054	1.042	18.44	304.6	0.98	0.0038
0.079	4.416	30.32	671.1	4.39	0.0012
0.056	1.297	20.11	353.75	1.02	0.077

Table 13: Model comparison between quadratic and linear-quadratic predictions and squared errors.

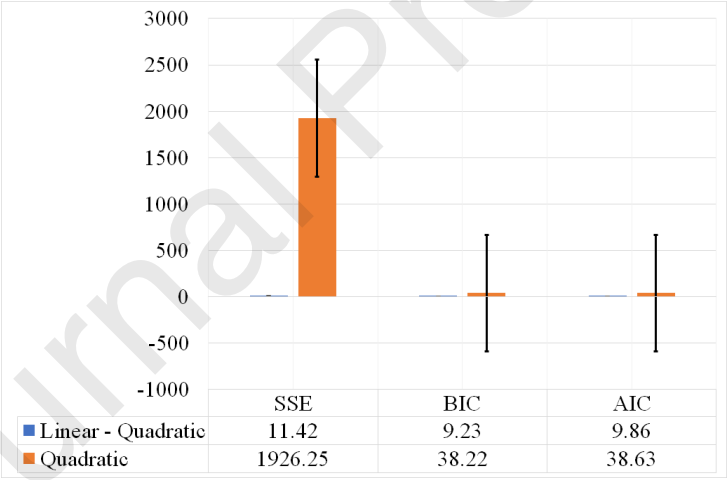

Figure 24: Information criteria (AIC / BIC).

The linear-quadratic model has a lower SSE and significantly lower AIC and BIC values, indicating a better fit. Thus, all three criteria show that this model is the most suitable for representing the six structura adhesives,

Journal Pre-proof

offering the best compromise between accuracy and complexity.

5.6. Statistical Analysis of Adhesive Mechanical Properties

Based on Fig. 16, ANOVA and Kruskal-Wallis tests were performed to evaluate whether the differences in E_v, ν_v, and ζ among the adhesives are statistically significant, as indicated in Table 14.

Property	ANOVA p-value	Kruskal-Wallis p-value	Significant differences
E_v	2.02×10^{-24}	4.77×10^{-5}	Yes (ANOVA)
ν_v	0.00618	0.0181	Yes (ANOVA)
ζ	2.45×10^{-15}	3.37×10^{-4}	Yes (ANOVA)

Table 14: Statistical analysis of mechanical properties using ANOVA and Kruskal-Wallis tests.

The very low p-values from both ANOVA and Kruskal-Wallis tests indicate statistically significant differences between groups for E_v, ν_v, and ζ. This confirms that the mechanical properties vary significantly among the structural adhesives analyzed.

5.7. Comparative Analysis of Adhesive Behavior Based on Tg, Damping, and Crosslink Density

The analysis highlights distinct adhesive behaviors, primarily driven by the glass transition temperature (T_g) relative to the testing temperature (25 °C), and by their mechanical response under dynamic excitation (viscoelastic fit).

1. **Sicomin SC** has a T_g well above the test temperature (Table 9). It aligns with the fit trend (near-zero residual, Fig. 13) and exhibits an

Journal Pre-proof

almost purely elastic response. Its high crosslink density significantly restricts segmental motion, limiting energy dissipation even under vibration. While it falls within the fit domain, it lies on the edge of the main data cluster—indicating marginal viscoelasticity. Furthermore, in the low-frequency regime, Sicomin clearly deviates from the fit in the first mode (Fig. 25a) and only begins to approach it by the second mode (Fig. 25b), confirming its borderline behavior in the high-frequency fit. The coefficient of determination R^2 (see Fig. 25a) shows that the viscoelastic behavior is better captured in the high-frequency regime. The fit around the mode 2 appears satisfactory from a visual standpoint, as shown in Fig. 25b, but the damping does not satisfy the low-damping condition ($\zeta < 0.1$) used in the study, as illustrated in Fig. 22.

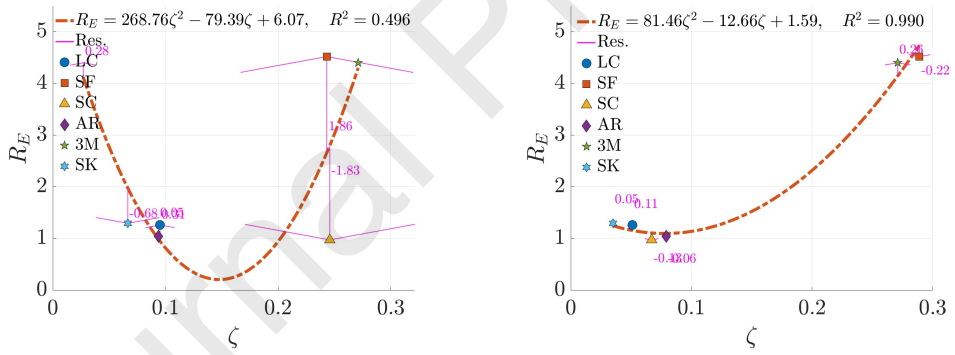

(a) Fit – Mode 1

(b) Fit – Mode 2

Figure 25: Quadratic fit and residuals of the Young's modulus ratios for the adhesive set as a function of damping factor at low frequency (adhesive names are abbreviated).

2. **3M 2216**, with a T_g close to the testing temperature, also fits well (low residual), but with a notably damped response. This intermediate state between glassy and rubbery phases allows limited chain mobility,

Journal Pre-proof

sufficient for moderate viscoelastic damping under dynamic excitation.

3. **Loctite, Araldite, and Sikadur 30** have T_g values below the testing temperature. They lie close to the fit curve with low residuals and moderate damping. Their stabilized chain mobility results in typical viscoelastic behavior with limited energy dissipation.
4. **SAF 30**, despite having a T_g near 25 °C and moderate damping, lies outside the fit (Fig. 13). This deviation may stem from a dynamic response not well captured by the model or from dissipation mechanisms beyond the model's scope. Interestingly, even Sicomin—despite being nearly elastic—remains within the fit, highlighting model limitations and suggesting the need to account for additional factors such as molecular structure or network homogeneity.

These results suggest that T_g position, excitation frequency, and crosslink density (as reflected in the coefficient e_2) are not sufficient alone to predict viscoelastic behavior.

5.8. Limitations of the model

The adhesives used do not represent the full range of products available on the market, these six samples reflect the formulations commonly used in industrial applications, particularly in the aerospace, automotive, civil engineering and marine sectors. This selection could therefore represent the viscoelastic behaviour of structural adhesives in general. However, the absence of certain families of adhesives limits the scope of the results.

The quality of the fit in Fig. 13 is good, with a coefficient of determination of $R^2 = 0.991$, indicating that the model explains nearly all of the variance

Journal Pre-proof

in the data. The 95% confidence bands represent the region where the true mean value of the model is likely to lie with 95% confidence. The confidence intervals (CI) are calculated based on the residual variance and the position of the points along the abscissa axis ζ):

Coefficient	Estimated value	95% CI
e_2	3585.4320	[-2559.878, 1366.510]
e_1	-340.9555	[-610.680, 3315.708]
e_0	8.9348	[-348.912, 3577.476]

Table 15: Quadratic model coefficients and 95% confidence intervals.

Although R^2 is very high, adhesive SAF 30 is slightly outside the confidence bands. This does not invalidate the overall quality of the fit: the model provides a visually good fit, but its stability is limited.

The confidence intervals are very wide, indicating that the model is not well-determined with only six . The large separation between the lower and upper bounds shows that the fit is highly sensitive to data variations. Confidence intervals including zero for all coefficients imply that the data alone are insufficient to robustly confirm the quadratic form.

Future work should include an expanded sample base to validate the observed behaviours.

6. Conclusion and Perspectives

This study presents a robust method for identifying the Young's moduli and Poisson's ratios of structural adhesives using resonant ultrasonic vibration (RUV) and validating them through non-contact laser vibrometry. A

Journal Pre-proof

combined experimental–numerical approach, based on RUV and 3D FEM analysis, enabled accurate estimation of elastic and damping properties for six adhesives (epoxy, methacrylate, and polyurethane). The FEM model proved essential for handling complex specimen geometries and extending analysis into high-frequency regimes.

A key contribution is the development and validation of a quadratic damping model grounded in the Kelvin–Voigt representation and the Doi–Edwards theory for entangled polymers. This model captures the nonlinear relationship between damping and storage modulus and was validated above 200 kHz, where strain rates are high. Among the tested adhesives, Sikadur 30 showed the highest stiffness, while 3M Scotch-Weld 2216 B/A exhibited the greatest damping capacity. The results support practical adhesive selection for structural applications involving dynamic or impulsive loading.

The determination of the glass transition temperature (T_g)—a parameter intrinsically linked to the elastic behavior of polymeric adhesives—allowed a more accurate interpretation of the low Young's modulus values obtained, particularly for the most compliant materials.

In this work, the effects of frequency-dependent damping and temperature were considered in the analysis. To further enhance the results, future research should aim to establish a manufacturing process capable of rigorously controlling porosity during adhesive sample preparation, while also investigating in detail the microscopic mechanisms governing adhesive crosslinking. To ensure the quality and robustness of the model, a broader representation of adhesives should be used.

Journal Pre-proof

7. Acknowledgments

Serges Kikwani gratefully acknowledges financial support from the French Government Scholarship Program (Bourse du Gouvernement Français – BGF). We also thank Jean-Laurent Gardarein and Nathalie Ehret from IUSTI (Marseille, France) for helping us with the use of the helium pycnometer and the differential scanning calorimetry (DSC) equipment.

Appendix A. Development of the Relationship: $E_0 = k_0 E_{\text{static}}$

1. Definitions

- E_{static}: Static (plateau) Young's modulus at long timescales, associated with entanglement effects.
- E_0: Intrinsic (high-frequency) modulus representing local chain elasticity or segmental response.
- G^0: Intrinsic shear modulus.
- G_n^0: Plateau shear modulus due to polymer entanglements. At Zero Frequency ($\omega \to 0$): The dynamic modulus reduces to the static (equilibrium) modulus:

$$\lim_{\omega \to 0} G'(\omega) = G_e \quad \text{(equilibrium modulus)}.$$

For compressible polymers, these are related to the intrinsic Young's modulus via Poisson ratio ($0 < \nu < 0.5$):

$$E_0 = 2(1+\nu)G^0, \quad E_{\text{static}} = 2(1+\nu)G_e.$$

Journal Pre-proof

Journal Pre-proof

2. Modulus Scaling from Doi-Edwards Tube Theory [48]

From polymer physics:

$$G_n^0 \sim \frac{k_B T}{L_e^3}, \quad G^0 \sim \frac{k_B T}{l_p^3}$$

where:

- k_B is the Boltzmann constant,
- L_e: Entanglement length,
- l_p: Persistence length,
- T is the absolute temperature.

Taking the ratio:

$$\frac{G^0}{G_n^0} \sim \left(\frac{L_e}{l_p}\right)^3$$

Therefore, the ratio of moduli becomes:

$$\frac{E_0}{E_{\text{static}}} = \frac{G^0}{G_n^0} \sim \left(\frac{L_e}{l_p}\right)^3$$

3. Final relationship

$$E_0 = k_0 E_{\text{static}}, \quad \text{where} \quad k_0 \sim \left(\frac{L_e}{l_p}\right)^3.$$

Journal Pre-proof

Appendix B. SOLID WORKS Mold dimension

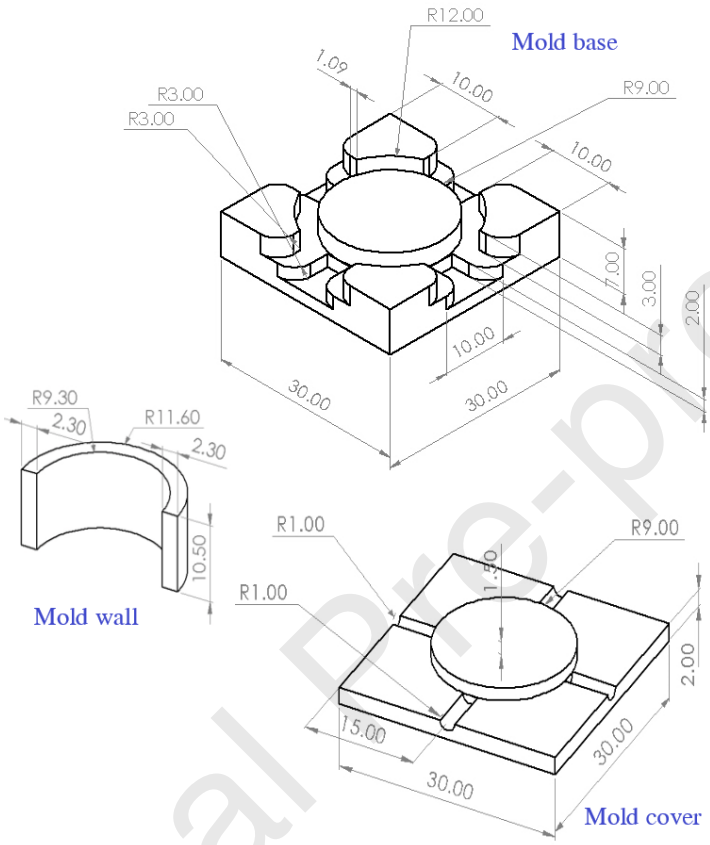

Figure B.26: 3D SOLID WORKS Mold dimension in mm.

Appendix C. Appendix: Implementation Details of the Inversion Procedure in MATLAB R2024a and COMSOL Multiphysics 6.1

A.1 Inversion Setup and Parameters

- **Optimization algorithm:** Nelder–Mead, implemented via `fminsearchbnd`, an extended version of `fminsearch` that supports bound constraints.

Journal Pre-proof

- **Estimated parameters:**
  - Young's modulus E : Within the range $[400, 3000]$ MPa for Saf 30, $[4000, 6000]$ and MPa and 3M2216, $[10000, 16000]$ MPa for Sikadur 30. (See Table 8)
  - Poisson's ratio ν : Within the range $[0.29, 0.40]$. (See Table 8)
- **Initial guess:**
  - Young's modulus E : Provisionnal Young moduli values (See Fig. 9.)
  - Poisson's ratio ν : Provisionnal Poisson ratio values. (See Fig. 6)
- **Constraints:** Soft bounds applied via `fminsearchbnd` to ensure physically admissible values.
- **Multi-start strategy:** Not applied; a single initialization was used in this study.Problem is well-posed over the interval in which the solutions are sought [25].

A.2 Convergence Settings

The convergence criteria and solver options used during optimization are as follows:

- **Objective function tolerance:** `TolFun` $= 10^{-3}$.
- **Parameter tolerance:** Default value from `fminsearchbnd`.
- **Output display:** Iterative display enabled, along with convergence plot (`optimplotfval`).

Journal Pre-proof

Journal Pre-proof

- **Maximum number of iterations:** Not explicitly specified; default values were used.

A.3 Objective Function

The objective function `Modelo_ok2(x)` performs the following steps:

1. Updates the input parameters in the COMSOL model,
2. Runs the simulation via the LiveLink interface,
3. Computes the squared error between simulated and experimental results.

A.4 Summary of Parameters (Araldite Adhesive)

Numerical Setting	**Value / Description**
Optimization algorithm	Nelder–Mead (`fminsearchbnd`)
Estimated parameters	E, ν
Parameter bounds	$E \in [400, 6000]$ MPa, $\nu \in [0.29, 0.40]$
Initial values	$E = 4900$ MPa, $\nu = 0.33$
Objective tolerance	10^{-3}
Parameter tolerance	Default
Output display	Iterative + convergence plot
Multi-start strategy	Not used

Table C.16: Summary of numerical settings for the parameter inversion (Araldite Adhesive).

Journal Pre-proof

References

[1] A. Maurel-Pantel, M. Voisin, F. Mazerolle, and F. Lebon. Comparison of three different adhesive joints using static and dynamic impact tests: Development of a new drop weight impact test rig incorporating a modified arcan fixture. *International Journal of Adhesion and Adhesives*, 114:103104, 2022.

[2] C. Yildirim, H. Ulus, H.S. Sas, S. Topal, and M. Yildiz. Assessing the fracture and dynamic mechanical performance of cf/pekk joints bonded with epoxy-based adhesive film for aerospace applications: Impact of thermal and cycling hygrothermal conditions. *Composites Part A: Applied Science and Manufacturing*, 190:108659, 2025.

[3] M. Lamberti, A. Maurel-Pantel, F. Ascione, and F. Lebon. Influence of web/flange reinforcement on the gfrp bonded beams mechanical response: A comparison with experimental results and a numerical prediction. *Composite Structures*, 147:247–259, 2016.

[4] F. Ramezani, B.D. Simões, R.J.C. Carbas, E.A.S. Marques, and L.F.M. da Silva. Developments in laminate modification of adhesively bonded composite joints. *Materials*, 16(2):568, 2023.

[5] T. Topkaya and M.Y. Solmaz. Fatigue behavior of honeycomb sandwich composites under flexural and buckling loading. In *International Conference on Advanced Materials and Systems (ICAMS)*, pages 177–182. The National Research & Development Institute for Textiles and Leather-INCDTP, 2016.

Journal Pre-proof

[6] T. Topkaya and M.Y. Solmaz. Investigation of low velocity impact behaviors of honeycomb sandwich composites. *Journal of Mechanical Science and Technology*, 32:3161–3167, 2018.

[7] L.D.R. Grant, R.D. Adams, and L.F.M. da Silva. Effect of the temperature on the strength of adhesively bonded single lap and t joints for the automotive industry. *International journal of adhesion and adhesives*, 29(5):535–542, 2009.

[8] M. A. Musthaq, H.N. Dhakal, Z. Zhang, A. Barouni, and R. Zahari. The effect of various environmental conditions on the impact damage behaviour of natural-fibre-reinforced composites (nfrcs)–a critical review. *Polymers*, 15(5):1229, 2023.

[9] K. Takagi, S. Kamo, K. Hasegawa, T. Matsumoto, T. Nishino, and A. Takahara. Development of destructive surface modification of peek (poly ether ether ketone) for high adhesion strength. *Mitsubishi juko giho*, 58:1–7, 2021.

[10] K. Idrissa, A. Maurel-Pantel, F. Lebon, and N. Guermazi. On the durability performance of two adhesives to be used in bonded secondary structures for offshore wind installations. *Materials*, 17(10):2392, 2024.

[11] R. Niu, Y. Yang, Z. Liu, Z. Ding, H. Peng, and Y. Fan. Durability of two epoxy adhesive bfrp joints dipped in seawater under high temperature environment. *Polymers*, 15(15):3232, 2023.

[12] A. Billon. *Méthode d'évaluation non-destructive de la qualité du collage*

Journal Pre-proof

des composites de renforcement pour le génie civil. PhD thesis, Université Paris-Est, 2016.

[13] M. Lamberti, Aurelien Maurel-Pantel, K. Idrissa, and F. Lebon. Porosity estimation of a micro-cracked adhesive interface by μct scanning: Comparison between experimentally measured effective stiffnesses and those predicted by an imperfect interface model. *International Journal of Adhesion and Adhesives*, 131:103653, 2024.

[14] Ed ASTM. Standard test method for dynamic young's modulus, shear modulus, and poisson's ratio by impulse excitation of vibration. *Annual Book of ASTM Standards*, 3:1876, 1876.

[15] M. Alfano and L. Pagnotta. A non-destructive technique for the elastic characterization of thin isotropic plates. *Ndt & E International*, 40(2):112–120, 2007.

[16] D. Laporte. *Analyse de la réponse d'assemblages collés sous des sollicitations en dynamique rapide. Essais et modélisations*. PhD thesis, ISAE-ENSMA Ecole Nationale Supérieure de Mécanique et d'Aérotechique-Poitiers, 2011.

[17] R. Medina and A. Bayón. Elastic constants of a plate from impact-echo resonance and rayleigh wave velocity. *Journal of Sound and Vibration*, 329(11):2114–2126, 2010.

[18] J.J. Wang, T.P. Chang, B.T. Chen, and H. Wang. Determination of poisson's ratio of solid circular rods by impact-echo me thod. *Journal of Sound and Vibration*, 331(5):1059–1067, 2012.

Journal Pre-proof

[19] R.J.C. Carbas, E.A.S. Marques, L.F.M. Da Silva, and A.M. Lopes. Effect of cure temperature on the glass transition temperature and mechanical properties of epoxy adhesives. *The Journal of Adhesion*, 90(1):104–119, 2014.

[20] R.C. Jacques, L.A. Corrêa, C.A. Ferreira, and T.G.R. Clarke. Correlation between electromechanical impedance and thermal analysis for adhesive cure time evaluation in shm gw applications. *Materials Research*, 27:e20240313, 2024.

[21] Y. Y. Lim, ST Smith, and I. Izadgoshasb. Smart-based monitoring of epoxy using piezoelectric transducers. *Proceedings of the SHMII*, 2017.

[22] R. Benlachemi, E. Ogam, N. Ongwen, A. Boudour, and Z. E. A. Fellah. Investigating the young's modulus of cu-al-be shape memory alloy using a phase diagram, vibration spectroscopy and ultrasonic waves. *Journal of Alloys and Compounds*, 976:173010, 2024.

[23] D. Chanbi, L. Adnane Amara, E. Ogam, S. E. Amara, and Z. E. A. Fellah. Microstructural and mechanical properties of binary Ti-rich Fe–Ti, Al-rich Fe–Al, and Ti–Al alloys. *Materials*, 12(3):433, 2019.

[24] D. Chanbi, E. Ogam, S. E. Amara, and Z. E. A. Fellah. Synthesis and mechanical characterization of binary and ternary intermetallic alloys based on Fe-Ti-Al by resonant ultrasound vibrational methods. *Materials*, 11(5):746, 2018.

[25] E. Ogam, A. Wirgin, S. Schneider, Z.E.A. Fellah, and Y. Xu. Recovery

Journal Pre-proof

of elastic parameters of cellular materials by inversion of vibrational data. *Journal of Sound and Vibration*, 313(3-5):525–543, 2008.

[26] A. Tirella, G. Mattei, and A. Ahluwalia. Strain rate viscoelastic analysis of soft and highly hydrated biomaterials. *Journal of Biomedical Materials Research Part A*, 102(10):3352–3360, 2014.

[27] G. Ogam, J.P. Groby, and E. Ogam. A non-linear vibration spectroscopy model for structures with closed cracks. *International Journal of Non-Linear Mechanics*, 59:60–68, 2014.

[28] J. Ewins, D.˙ *Modal Testing: Theory, Practice and Application*. John Wiley & Sons, Chichester, UK, 2 edition, 2000.

[29] Xinzong Wang, Xiaofang Kang, Ling Ji, Ao Zhang, and Guanghui Xia. Low frequency vibration energy harvesting of bio-inspired multi-stable piezoelectric vibration system with an adjustable device. *Chaos, Solitons & Fractals*, 192:116026, 2025.

[30] F. Cottone, H. Vocca, and L. Gammaitoni. Nonlinear energy harvesting. *Physical review letters*, 102(8):080601, 2009.

[31] A. Erturk and D. J. Inman. *Piezoelectric energy harvesting*. John Wiley & Sons, 2011.

[32] S. C. Stanton, C. C. McGehee, and B. P. Mann. Nonlinear dynamics for broadband energy harvesting: Investigation of a bistable piezoelectric inertial generator. *Physica D: Nonlinear Phenomena*, 239(10):640–653, 2010.

Journal Pre-proof

Journal Pre-proof

[33] M. Bordes. *Etude du vieillissement de liaisons adhésives en milieu marin pour application offshore*. PhD thesis, Insa Lyon, 2009.

[34] J Aucher, B Vieille, and L Taleb. Etude comparative de l'influence de la température sur le comportement de stratifiés tissés carbone à matrice thermodurcissable ou à matrice thermoplastique. *Marseille, France*, pages 24–28, 2009.

[35] P. Weiss. La chimie des polymères. *Université Médicale Virtuelle Francophone*, 2010.

[36] M. Verdet, A. Cointe, J.L. Coureau, P. Galimard, C. Delisée, and A. Salenikovich. Caractérisation des adhésifs et des performances de goujons-collés sous chargement thermique. *Academic Journal of Civil Engineering*, 34(1):204–211, 2016.

[37] Dassault Systèmes. SolidWorks Simulation Software. `https://www.solidworks.com/`, 2025. Version used: SolidWorks 2025.

[38] COMSOL Inc. Comsol multiphysics, version 6.1.0.357, 2022.

[39] Dassault Systèmes. *ABAQUS 2022 Documentation*. Dassault Systèmes Simulia Corp., Providence, RI, USA, 2022. Version 2022.

[40] J.A. Nelder and R. Mead. A simplex method for function minimization. *The Computer Journal*, 7(4):308–313, 1965.

[41] MATLAB. *version 9.13.0 (R2024a)*. The MathWorks Inc., Natick, Massachusetts, https://www.mathworks.com., 2024.

Journal Pre-proof

[42] M. Al-Zu'bi, L. Anguilano, and M. Fan. Effect of incorporating carbon- and silicon-based nanomaterials on the physico-chemical properties of a structural epoxy adhesive. *Polymer Testing*, 128:108221, 2023.

[43] Mohsen Barzegar, Yevgeniya Lugovtsova, J. Bulling, T. Mishurova, D. J. Pasadas, A. L Ribeiro, and H. G Ramos. Adhesive porosity analysis of composite adhesive joints using ultrasonic guided waves. *IEEE Transactions on Ultrasonics, Ferroelectrics, and Frequency Control*, 71(4):485–495, 2024.

[44] W.E. Guin, J.V. Bausano, A. N. Taets, A. T. Nettles, and S. Ragasa. Characterization of fracture behavior in adhesively bonded joints with porosity in the adhesive layer using x-ray computed tomography. *Composites Science and Technology*, 261:111025, 2025.

[45] Hui W., Guodong K., Yizhe C., Zhaoyi L., and Lin H. Reducing interface defects and porosity of adhesive bonded aluminum alloy joints via ultrasonic vibration. *Polymers*, 15(9):2098, 2023.

[46] ASTM International. Standard test method for density of solid pitch (helium pycnometer method). `https://www.astm.org/d4892-89r04.html`, 2024. ASTM D4892-24.

[47] J. Carcione. *Wave fields in real media: Wave propagation in anisotropic, anelastic, porous and electromagnetic media*, volume 38. Elsevier, 2007.

[48] M. Doi and S.F. Edwards. *The Theory of Polymer Dynamics*. International series of monographs on physics. Clarendon Press, 1988.

Journal Pre-proof

[49] J. D Ferry. *Viscoelastic properties of polymers*. John Wiley & Sons, 1980.

Journal Pre-proof

Journal Pre-proof

Declaration of interests

☒ The authors declare that they have no known competing financial interests or personal relationships that could have appeared to influence the work reported in this paper.

☐ The authors declare the following financial interests/personal relationships which may be considered as potential competing interests:

Journal Pre-proof